AD-A108 123 FOREIGN TECHNOLOGY DIV WRIGHT-PATTERSON AFB OH F/G 20/4
ACTA MECHANICA SINICA (SELECTED ARTICLES).(U)
OCT 81
UNCLASSIFIED FTD-ID(RS)T-0707-81 NL

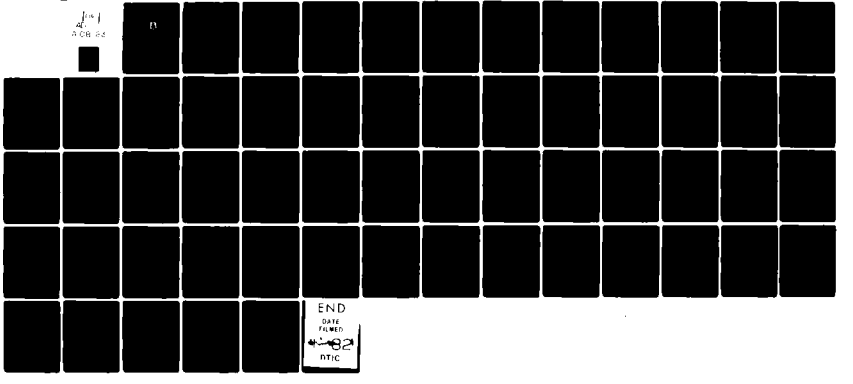

END
DATE FILMED
1-82
DTIC

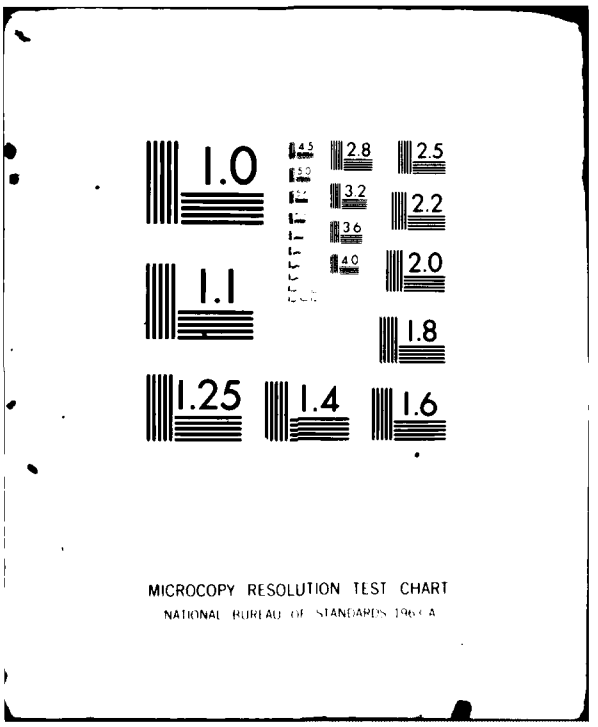
1.0
1.1
1.25
1.4
1.6
1.8
2.0
2.2
2.5
2.8
3.2
3.6
4.0
4.5
5.0
MICROCOPY RESOLUTION TEST CHART
NATIONAL BUREAU OF STANDARDS 1963 A

FTD-ID(RS)T-0707-81

FOREIGN TECHNOLOGY DIVISION

ACTA MECHANICA SINICA
(Selected Articles)

Approved for public release;
distribution unlimited.

EDITED TRANSLATION

FTD-ID(RS)T-0707-81 29 October 1981

MICROFICHE NR: FTD-81-C-000989

ACTA MECHANICA SINICA (Selected Articles)

English pages: 56

Source: Acta Mechanica Sinica, Nr. 4, 1979, pp. 303-322, 344-352

Country of origin: China
Translated by: SCITRAN
F33657-78-D-0619
Requester: FTD/TQTA

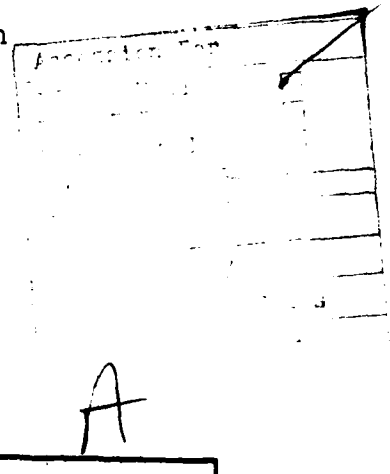

A

PREPARED BY:

TRANSLATION DIVISION
FOREIGN TECHNOLOGY DIVISION
WP-AFB, OHIO.

TABLE OF CONTENTS

GENERALIZED VARIATIONAL PRINCIPLES, VARIATIONAL PRINCIPLES AND DUAL EXTREMUM PRINCIPLES OF GASDYNAMICS FOR THE DIRECT PROBLEM OF TURBOMACHINE AIRFOIL CASCADES ON AN ARBITRARY STREAM SHEET OF REVOLUTION*[1)]

Liu Gao-Lian

ABSTRACT

The present paper is devoted to the search for variational principles for the direct aerodynamic problem of channels and aerofoil cascades (with prescribed distributed mass injection or/and suction along the profile contours for blade cooling or boundary layer control) on an arbitrary stream sheet of revolution and aimed mainly at providing a rigious and sound theoretical basis for introducing and widely applying the finite element method to computational aerodynamics of turbomachines. Three generalized variational principles (among which two are for homoentropic flow, and the other for nonhomoentropic flow) are developed first, and then from them three families of variational principles are derived respectively by means of successive transformations. Furthermore, for homoentropic subsonic flows a pair of dual extremum principles are also shown to exist.

Special attention is payed to taking full advantage of 2 effective means: "natural boundary conditions" and "artificial boundaries", in order to greatly simplify the numerical treatment of various boundary conditions characterizing the complexitg of the cascade problem. So in all variational principles all boundary conditions have been converted to natural ones.

The variational principles presented here can be used to advantage as basis also for variational-finite difference method and for various direct variational methods (e.g. Ritz's method, Kantorovich's method etc.).

---

* received on February 26, 1978.

1) This paper has been presented in the National Experience Exchange Meeting in the thermodynamic calculation, design and experiment of the aerodynamics of turbomachines.

2) Author's present address: Shanghai Mechanics Institute.

This paper is devoted to the investigation of the variational principles for the direct problem of channel and airfoil cascade aerodynamics on an arbitrary stream sheet of revolution (with gas injection and/or suction along the profile contour of the blade. For example, boundary layer control, gas film or perspiration type of cooling, etc.) in order to provide a more rigorous theoretical basis for the introduction and expansion of the finite element method in the field of turbomachine aerodynamic calculation. The results include: 1. For homoentropic flow, two variational principles were established, and then from them two families of semi-generalized variational principles, including a pair of dual extremum principles under subsonic condition were derived; 2. For nonhomoentropic flow, a generalized variational principle was established and then from it a family of sub-generalized variational principles was derived. This paper placed special emphasis on taking full advantage of the natural boundary conditions and artificial boundaries to simplify the treatment of various boundary conditions of the complex cascade problem. In addition to being in the finite element method, they can be used to create advantageous conditions for the variational-finite difference method and for various direct variational methods.

The use of the variational principle to describe a physical process has the unique advantage of simple straight forwardness. It can use its unique natural boundary conditions to simplify (including on the discontinued surface) the treatment of boundary conditions. It has always been the basis of various direct variational methods. The generalized variation principle emerged in the fifties [1]. It created conditions to simplify the selection of coordinate functions as well as to increase the accuracy in the direct variation method. It has been primarily used in solid state mechnaics. The investigation and applications of the variational principl- in fluid mechanics have been rare [3-6]. Its major reasons most probably are the complexity of the boundary

conditions (especially in the case of cascades) and the nonlinearity of the problem. In the recent decade, the development of the finite element method brought new interest to the classical variational principles. The variational principle is one of the theoretical foundations of the finite element method. The characteristics of the finite element method (e.g., arbitrary slicing and slice implantation) also greatly overcomes the difficulties encountered in the treatment of the complicated boundary conditions using the direct variational method. Thus, it eliminated the disadvantage that such a method was only suitable for the general characteristics, but not suitable for the field distribution. Therefore, the combination of the two methods is really complementary.

This paper for the first time established the variational principles, the variational principle families and the dual extremum principles of gas dynamics for the directproblem of cascades and channels of turbomachines on an arbitrary stream sheet of revolution. Taking into account the needs of the newly developed area (such as boundary layer control, gas film or perspiration type of cooling, etc.), we have included the conditions of direct problems with gas injection and suction on the surface of the blade. To further simplify the treatment of the boundary conditions , special attention was paid to fully take advantage of the unique actions of the natural boundary conditions and the artificial boundaries. The latter enabled us to reach a better coordination on the intersection of each element in the finite element method. In the classical direct method, it was possible to select coordination functions more flexibly by area, which simultaneously assured the continuity on the artificial boundary to the extent possible.

I. The gas dynamic equations of cascades on an arbitrary stream sheet of revolution

We limited our investigation to the condition that the generalized enthalpy $\bar{H}$ (also known as the stagnant evolution enthalpy) of the incoming flow is homogeneous (i.e., $\bar{\nabla}_{\rho} H = 0$). Here $H = i + (w^2/2) - (u^2/2)$ and $\bar{\nabla}$ represents the gradient along the surface of the flow. Therefore, for a system rotating at a constant angular velocity ω_{γ}, the gas dynamic equations [7] for an ideal gas flowing along an arbitrary stream sheet of revolution under steady and adiabatic conditions can be written in the following dimensionless forms (Figure 1):

1. Homoentropic flow (Figure 2(b)

Under this condition, $\bar{\nabla}H = \bar{\nabla}S \equiv 0$. The gas dynamic equations are:

$$\frac{\partial(\tau r \bar{\rho} \Lambda_l)}{\partial l} + \frac{1}{r}\frac{\partial(\tau r \beta \Lambda_\varphi)}{\partial \varphi} = 0 \qquad (1a)$$

$$\frac{\partial \Lambda_l}{\partial \varphi} - \frac{\partial[(\Lambda_\varphi + \Lambda_u)r]}{\partial l} = 0 \qquad (1b)$$

$$\bar{\rho} = \bar{a}^{1/m} = \bar{p}^{1/\kappa} = \left\{1 - \frac{1}{2m}(\Lambda^2 - \Lambda_*^2)\right\}^m \qquad (1c)$$

where $\Lambda = w/a_0$, $\Lambda_\varphi = w_\varphi/a_0$, $\Lambda_l = w_l/a_0$, $\Lambda_u = \omega r/a_0 = u/a_0$, $\bar{\rho} = \rho/\rho_0$, $\bar{p} = p/p_0$, $\bar{a} = a/a_0$, $a_0^2 = c_p T_0/m = H/m$, $m = 1/(\kappa - 1)$, w, ρ, p, T, and a represent relative flow velocity, density, pressure, temperature and speed of sound, respectively; the subscript 0 represents the parameters of point 0 in Figure 2(b); c_p and k are the isobaric specific heat and thermal insulation coefficient, respectively. All the linear dimensions used are the ratios with respect to the width B in the l direction of the cascade; τ is the thickness of the flowing layer.

From Equations (1a) and (1b), one can introduce a flow function ψ and "position" function Φ as follows:

$$\partial\psi/\partial\varphi = \tau r \beta \Lambda_l, \quad \partial\psi/\partial l = -\tau r \bar{\rho} \Lambda_\varphi \qquad (1d)$$

$$\partial\Phi/\partial l = \Lambda_l, \quad \partial\Phi/\partial\varphi = (\Lambda_\varphi + \Lambda_u)r \qquad (1e)$$

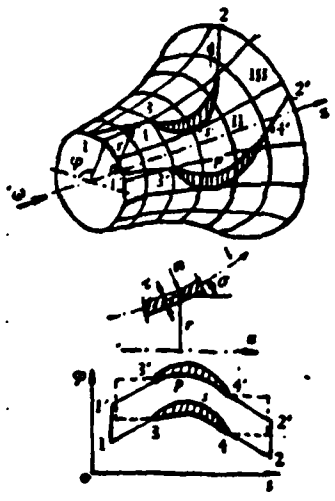

Figure 1. Cascade on an arbitrary stream sheet of revolution. Reference lines $\overline{13}$ and $\overline{42}$ can be selected arbitrarily as indicated by the dotted lines.

Please note that the presence of the function ϕ does not necessarily mean that the flow is rotationless. It only indicates that the component of the absolute degree of revolution $\nabla \times c$ perpendicular to the flow direction is zero which means that the flow surface coincides with the revolution surface.

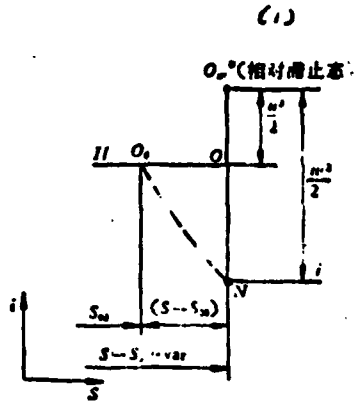

Figure 2(a) Non-homoentropic flow (the state point N can move in the horizontal direction too)

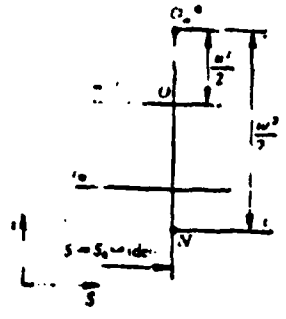

Figure 2(b) Homoentropic flow

Key: 1--relative stagnation state

2. Non-homoentropic flow (Figure 2(a)

Under the condition $\overline{\nabla}H \equiv 0$, but $\overline{\nabla}S \neq 0$ and $^{DS}/_{Dt} \neq 0$ (usually $^{DS}/_{Dt}$ is used to approximately consider the loss). At this time, the speed of sound a_o (and T_o) at point 0 in Figure 2(a) are constant in the entire flow field. The following dimensionless quantities are further supplemented in the following:

$$\tilde{p}_0 = p/p_{00},\quad \tilde{\rho}_0 = \rho/\rho_{00},\quad \bar{S} = S/R,\quad \tilde{S} = S/c_v = \bar{S}/m$$

The subscript ^{00} indicates that the parameters are for point 0_0 in Figure 2(a). Thus, the following gas dynamic equations [7] can be obtained:

$$\frac{\partial(\tau r\tilde{\rho}\Lambda_l e^{-\Delta\bar{S}})}{\partial l} + \frac{\partial(\tau\tilde{\rho}\Lambda_\varphi e^{-\Delta\bar{S}})}{\partial\varphi} = 0 \tag{2a}$$

$$\frac{\partial\Lambda_l}{\partial\varphi} - \frac{\partial[(\Lambda_\varphi + \Lambda_u)r]}{\partial l} = \frac{-m}{\varepsilon}\tau r\tilde{\rho}_0\frac{\partial(\Delta\bar{S})}{\partial\psi} \tag{2b}$$

$$\left.\begin{aligned}&\tilde{\rho} = \tilde{p}^{\frac{1}{\gamma}} = \tilde{a}^{2m} = \{1 - [(\Lambda^2 - \Lambda_u^2)/(2m)]\}^m\\ &\tilde{\rho}_0 = \tilde{\rho}\exp(-\Delta\bar{S})\\ &(\tilde{p}_0/\tilde{\rho}_0^\gamma)\exp(-\Delta\bar{S}) = 1\end{aligned}\right\} \tag{2c}$$

where the flow function ψ is defined by the following equations:

$$\left.\begin{aligned}&\partial\psi/\partial\varphi = \tau r\tilde{\rho}\Lambda_l e^{(-\Delta\bar{S})} = \tau r\tilde{\rho}_0\Lambda_l\\ &\partial\psi/\partial l = -\tau\tilde{\rho}\Lambda_\varphi e^{(-\Delta\bar{S})} = -\tau\tilde{\rho}_0\Lambda_\varphi\end{aligned}\right\} \tag{2d}$$

A generalized flow function Θ can be defined as:

$$\partial\Theta/\partial\varphi = \tau r\tilde{\rho}\Lambda_l,\quad \partial\Theta/\partial l = -\tau\tilde{\rho}\Lambda_\varphi \tag{2e}$$

and $\Delta\bar{S} = m\Delta\tilde{S} = \bar{S} - \bar{S}_{00}$ is usually given in the form of $\Delta\bar{S} = f(l,\psi)$.

As for the various boundary conditions, they will be given in the form of natural boundary conditions in the variational principles discussed in the following sections.

II. The generalized variational principles of the homoentropic flow

In the generalized variational principles, the variations of various gas dynamic parameters are independent. From this the boundary conditions of all the gas dynamic equations of cascades or channels on an arbitrary stream sheet of revolution can be automatically derived (including the continuity conditions on the artificial boundaries Σ).

(A) Generalized variational Principle I

The necessary condition for a general function J_1 which is equivalent to the solution of the homoentropic flow of a cascade with an arbitrary revolution stream sheet is: $\delta_{\mathcal{B}} J_1 = 0$.

Here, Λ_l, Λ_φ, ψ, $\tilde{\rho}$ and $\tilde{p}$ undergo independent variations. If we let $\Pi(\tilde{p}, \tilde{\rho}) = m\{(\tilde{p}/\varepsilon)[1 - \ln(\tilde{p}\tilde{\rho}^{-\varepsilon})] - \tilde{\rho}\}$ then,

$$J_1(\Lambda_l, \Lambda_\varphi, \psi, \tilde{p}, \tilde{\rho}) = \iint_{A} \left\{ \frac{\Lambda_l}{\tau r} \frac{\partial \psi}{\partial \varphi} - \frac{(\Lambda_r + \Lambda_a)}{\tau} \frac{\partial \psi}{\partial l} - \frac{\tilde{\rho}}{2}(\Lambda^2 - \Lambda_a^2) - \Pi \right\} \tau r \, d\varphi \, dl$$
$$+ \oint_{(c_3)} (\Lambda_m + \Lambda_a i_\varphi)\psi \cdot d\mathbf{S} + \oint_{(c_3)} (\Lambda + \Lambda_a i_\varphi)\{\psi - [\psi(l)]_m\} \cdot d\mathbf{S}$$
$$- \frac{1}{2}\int_{(c_2')} (\Lambda_+ + \Lambda_- + 2\Lambda_a i_\varphi)(\psi_+ - \psi_- - \Delta\psi_{1,2}) \cdot d\mathbf{S}$$
$$+ \frac{1}{2}\int_{(\Sigma)} (\psi_- - \psi_+)(\Lambda_+ + \Lambda_- + 2\Lambda_a i_\varphi) \cdot d\mathbf{S} \qquad \text{(I-1)}$$

where (A) represents the area of the region where solution is sought on the arbitrary stream sheet of revolution (i.e., the region 13422'4'3'1' in Figure 1); (Σ) represents the entire artificial boundaries (Figure 3); (c_1) represents the inlet surface $\overline{11'}$ and the outlet surface $\overline{22'}$ (Figure 1); (c_2) represents the boundary surfaces $\overline{13}$, $\overline{1'3'}$, $\overline{42}$ and $\overline{4'2'}$ in the periodic region in the front and back of the cascade; (c_2') represents the lower boundary surface $\overline{13}$ and $\overline{42}$; (c_3) represents the S and p surfaces along the profile contours of the blade; (c) represents the entire boundary, i.e., (c_1+c_2+c_3); the subscript + and - represent the the right and left side of the integration path, respectively); p_r represents the predicted quantity; "上" represents the upper boundary surface $\overline{13'}$ and $\overline{4'2'}$; " 下 " represents the lower boundary surface $\overline{13}$ and $\overline{42}$. In addition, $\Delta\psi_{1,2}$ represent the differences of ψ between $\overline{13}$ and $\overline{1'3'}$ and $\overline{42}$ and $\overline{4'2'}$, respectively:

$$\Delta\psi_{1,2} = \int_{\varphi}^{\varphi+\Delta\varphi} (\tau r \tilde{\rho} \Lambda_l)_{1,2} \, d\varphi \quad (\Delta\varphi \text{ represent angular pitch})$$

[Translators note: pages 1-6
上 = top and 下 = bottom.]

Apparently, $(\Delta\psi_2-\Delta\psi_1)$ is just equal to the amount of gas flow ejected from the profile contours of every blade.

Proof: Taking the variation of (I-1) and using the Green theorem, we get:

$$\delta J_1 = \iint_{(A)} \left\{\left(\frac{\partial[(\Lambda_\varphi+\Lambda_m)r]}{\partial l} - \frac{\partial\Lambda_l}{\partial\varphi}\right)\frac{\delta\psi}{\tau r} - \left(\frac{1}{\tau}\frac{\partial\psi}{\partial l}+q_\varphi\right)\delta\Lambda_\varphi \right.$$
$$\left. + \left(\frac{1}{\tau r}\frac{\partial\psi}{\partial\varphi}-q_l\right)\delta\Lambda_l - \left(\frac{\Lambda^2-\Lambda_m^2}{2}-\frac{\partial\Pi}{\partial\tilde{\rho}}\right)\delta\tilde{\rho} - \frac{\partial\Pi}{\partial\tilde{p}}\delta\tilde{p}\right\}\tau r\,d\varphi\,dl$$
$$+ \oint_{(c_1)}(\Lambda_{l,pr}-\Lambda_l)\delta\psi\,dS + \oint_{(c_2)}(\psi-\psi_{pr})\delta\Lambda_l\,dS$$
$$+ \frac{1}{2}\int_{(c_3')}\{(\delta\psi_+ + \delta\psi_-)(\Lambda_+-\Lambda_-) - (\psi_+ - \psi_- - \Delta\psi_{1,2})(\delta\Lambda_+ + \delta\Lambda_-)\}\cdot d\mathbf{S}_r$$
$$+ \frac{1}{2}\int_{(\Sigma)}\{(\delta\psi_+ + \delta\psi_-)(\Lambda_+-\Lambda_-) + (\psi_- - \psi_+)(\delta\Lambda_+ + \delta\Lambda_-)\}\cdot d\mathbf{S}$$

Key: 1,3,5,7--upper; 2,4,6,8--lower

Since all the variations are completely independent and arbitrary, therefore, the following set of conditions for an extremum can be obtained of $\delta J_1 = 0$:

Euler equations:

$$\left.\begin{array}{ll} \dfrac{\partial[(\Lambda_\varphi+\Lambda_m)r]}{\partial l} - \dfrac{\partial\Lambda_l}{\partial\varphi} = \cdot & \text{(extent of rotation)} \\ \partial\psi/\partial l = -\tau\tilde{\rho}\Lambda_\varphi,\ \partial\psi/\partial\varphi = \tau r\tilde{\rho}\Lambda_l & \text{(equivalent continuity equation)} \\ (\tilde{p}/\tilde{\rho}) + (\Lambda^2-\Lambda_m^2)/(2m) = 1 & \text{(energy equation)} \\ \tilde{p} = \tilde{\rho}^{(\varkappa)} & \text{(homoentropic relation)} \end{array}\right\} \quad \text{(I-2a)}$$

Natural boundary conditions:

for c_1: $\Lambda_\varphi = [\Lambda_\varphi(\varphi)]_{pr}$

for c_2: $\Lambda_{2,l} = \Lambda_{1,l}$ and $\psi_+ = \psi_- + \Delta\psi_{1,2}$

it can be deduced that on $\overline{13}$ and $\overline{1'3'}$ (as well as on $\overline{42}$ and $\overline{4'2'}$), all the gas dynamic parameters are equal (periodicity).

for c_3: $\psi_{1,\varphi} = [\psi_{1,\varphi}(l)]_{pr}$ (when there is no mass transfer on the surface of the blade, then $\psi_{s,p}$ = given constant).

for Σ: $(\Lambda_-)_l = (\Lambda_+)_l$ and $\psi_- = \psi_+$ from this one can deduce that all the gas dynamic parameters are continuous on Σ.

} (I-2b)

It has already assumed that $q = \tilde{\rho}A$ and the subscript t indicates the tangential component.

It is obvious here that from this generalized variational principle the solution to the homoentropic linear flow of a cascade ~~which~~ can satisfies ~~the~~ all the boundary conditions and is continuous ~~on the~~ at artificial boundary surface Σ. ~~can be obtained.~~

(B) Generalized variational Principle II

The necessary condition for a function J_{11} which is equivalent to the homoentropic flow solution of a cascade with an arbitrary stream sheet of revolution to have an extremum is: $\delta J_{11} = 0$.

Here Λ_1, $\Lambda_{\#}$, ϕ, $\tilde{p}$ and $\tilde{\rho}$ undergo independent variations

$$J_{11}(\Lambda_l, \Lambda_\varphi, \phi, \tilde{p}, \tilde{\rho}) = \iint_{(\Delta)} \left\{ q_l \frac{\partial \phi}{\partial l} + \frac{q_\varphi}{r} \frac{\partial \phi}{\partial \varphi} - \frac{\tilde{\rho}}{2} (\Lambda^2 + \Lambda_n^2 + 2\Lambda_n \Lambda_\varphi) + \Pi \right\} r\, dl\, d\varphi - \oint_{(\sigma_1+\sigma_2)} (q_n)_{ex} \phi r\, dS + \frac{1}{2} \int_{(\sigma_1')} (\phi_+ - \phi_- - \Delta\phi_{1,2})(q_+ + q_-) \cdot n_- r\, dS + \frac{1}{2} \int_{(\Sigma)} (\phi_+ - \phi_-)[q_+ + q_-] \cdot n r\, dS \qquad (II\text{-}1)$$

where n, t represent the unit vector in the outside normal and tangential directions of the integration path, respectively; $\Delta\phi_{1,2}$ represent the differences of ϕ on $\overline{13}$ and $\overline{1'3'}$ as well as $\overline{42}$ and $\overline{4'2'}$, respectively:

$$\Delta\phi_{1,2} = \int_{\varphi}^{\varphi+\Delta\varphi} [r(\Lambda_\varphi + \Lambda_n)]_{1,2} d\varphi$$

Proof: Taking the above variations and from $\delta J_{II}=0$, the following set of necessary conditions for an extremum can be obtained:

Euler equations:

$$\left.\begin{aligned} &\frac{\partial(\tau r q_l)}{\partial l} + \frac{\partial(\tau q_\varphi)}{\partial \varphi} = 0 && \text{(continuity equation)} \\ &\partial\phi/\partial l = \Lambda_l,\ \partial\phi/\partial\varphi = r(\Lambda_\varphi + \Lambda_u) && \text{(equivalent rotational degree function)} \\ &\left(\frac{\tilde{p}}{\tilde{\rho}}\right) + (\Lambda^2 - \Lambda_u^2)/(2m) = 1 && \text{(energy equation)} \\ &\tilde{p} = \tilde{\rho}^{(\kappa)} && \text{(homoentropic relation)} \end{aligned}\right\} \quad \text{(II-2a)}$$

Natural boundary conditions:

$$\left.\begin{aligned} &\text{for on } c_1 \not\subset:\ q_l = [q_l(\varphi)]_{c_1} \\ &\text{for on } c_2 \not\subset:\ q_{\nu c_2} = q_{\tau c_2} \quad \text{and} \quad \phi_{t_2} = \phi_{\tau_2} + \Delta\phi_{c_2} \\ &\text{from these one can deduce that all the gas dynamic parameters are equal (periodicity)} \\ &\text{for on } c_3 \not\subset:\ q_{c_3} = [q_{c_3}(l)]_{c_3} \quad \text{(where there is no mass transfer on the blade, } q_u = 0\text{)} \\ &\text{for on } \Sigma \not\subset:\ (q_+)_\Sigma = (q_-)_\Sigma \quad \text{and} \quad \phi_+ = \phi_- \\ &\text{from the above, we know that all the gas dynamic parameters are continuous} \end{aligned}\right\} \quad \text{(II-2b)}$$

It is apparent that from the generalized variational principle II, a solution to homoentropic flow of a cascade ~~which~~ can satisfies all the boundary conditions and is continuous ~~on the~~ at artificial boundaries ~~can be obtained~~ surface Σ.

III. Sub-generalized variational principle family of homoentropic flow

From the above generalized variational principles, a new series of variational principles can be derived (it can also be called the sub-generalized variational principles). The principle used here is based on that if the extremum conditions of a variational problem are applied to the original variational problem as constraints, then the solution of the extremum would not be changed [9]. The following examples show:

(A) The sub-variational principle family derived from J_1

(a) Substituting rows 2 and (4) in Equation (-2a) into J_1 and eliminating Λ_1, $\Lambda\varphi$ and $\tilde{p}$, we get the following variational principle:

$$J_1'(\psi, \tilde{\rho}) = \iint_{A_1} \left\{ \frac{1}{2r^2\tilde{\rho}} \left[\left(\frac{1}{r} \frac{\partial \psi}{\partial \varphi} \right)^2 + \left(\frac{\partial \psi}{\partial l} \right)^2 \right] - \frac{\Lambda_u}{r} \frac{\partial \psi}{\partial l} + \frac{\tilde{\rho}}{2} \Lambda_0^2 + m \left(\tilde{\rho} - \frac{\tilde{\rho}^{(a)}}{\varepsilon} \right) \right\} r \, dr \, d\varphi \, dl + \oint_{(a)} (\Lambda_{\varphi,m} + \Lambda_u) \psi \, dS + \oint_{(a)} \left(\Lambda_u i_\varphi \cdot t - \frac{1}{r\tilde{\rho}} \frac{\partial \psi}{\partial n} \right) \{ \psi - [\psi(l)]_m \} dS - \frac{1}{2} \int_{(a')} (\psi_2 - \psi_1 - \Delta\psi_{1,2}) \left\{ 2\Lambda_u i_\varphi \cdot t - \frac{1}{r} \left[\left(\frac{1}{\tilde{\rho}} \frac{\partial \psi}{\partial n} \right)_2 + \left(\frac{1}{\tilde{\rho}} \frac{\partial \psi}{\partial n} \right)_1 \right] \right\} dS + \frac{1}{2} \int_{(z)} (\psi_- - \psi_+) \left\{ 2\Lambda_u i_\varphi \cdot t - \frac{1}{r} \left[\left(\frac{1}{\tilde{\rho}} \frac{\partial \psi}{\partial n} \right)_+ + \left(\frac{1}{\tilde{\rho}} \frac{\partial \psi}{\partial n} \right)_- \right] \right\} dS \qquad (I'-1)$$

We only have to let $\delta J_1' = 0$ (assuming ψ and $\tilde{\rho}$ undergo variation independently) to obtain the first and third rows in Equation (I-2a) and Equation (I-2b).

(b) Substituting the third and fourth rows in Equation (I-2a) into J_1 and then eliminating $\tilde{p}$ and $\tilde{\rho}$ we get another subvariational principle:

$$J_1''(\psi, \Lambda_l, \Lambda_\varphi) = \iint_{A_1} \left\{ \frac{\Lambda_l}{\tau r} \frac{\partial \psi}{\partial \varphi} - \left(\frac{\Lambda_\varphi + \Lambda_u}{r} \right) \frac{\partial \psi}{\partial l} + \frac{X^{-m}}{\varepsilon} \right\} r \, dr \, d\varphi \, dl + L_1 \qquad (I''-1)$$

where $X = 1 - (\Lambda^2 - \Lambda_u^2)/(2m)$, L_1 represents the various linear integration terms in J_1.

Since $J_1'' = 0$ (let Λ, Λ_l vary independently with respect to $\Lambda\varphi$) we obtain the 1st and 2nd rows in equation (1-2a) and (1-2b).

(c) Using the 2nd, 3rd and 4th rows of equation (I-2a) as added constraints to J_1, we obtain the following variational principle III:

$$J_{III}(\psi) = \iint_{A_1} F_1 \cdot d\varphi \, dl + L_1 \qquad (III-1)$$

where $F_1 = \left[\frac{\tilde{\rho}}{\varepsilon} + \tilde{\rho}(\Lambda^2 + \Lambda_u \Lambda_\varphi) \right] \tau_2 - \frac{\tau r}{\varepsilon} \left| 1 + \frac{\Lambda_0^2}{2m} + \frac{\varepsilon + 1}{2} \Lambda^2 + \right.$ 1.1.1.

$$\times \left[1 - \frac{1}{2m}(\Lambda^2 - \Lambda_\infty^2)\right]^m$$

By letting $\delta J_{III} = 0$, the first equation of (I-2a) and Equation (I-2b) can be obtained.

(B) <u>The sub-generalized variational principle family derived from J_{II}</u>

Similar to the variational method used for J_I, we get:

(a) Sub-generalized variational principle

$$J'_{II}(\phi, \tilde{\rho}, \bar{\rho}) = \iint_{(A)} \left\{\frac{\tilde{\rho}}{2}\left[\left(\frac{\partial \phi}{\partial l}\right)^2 + \left(\frac{1}{r}\frac{\partial \phi}{\partial \varphi}\right)^2 - \frac{2\Lambda_\infty}{r}\frac{\partial \phi}{\partial \varphi}\right] + \Pi\right\} r\, dA\, d\varphi\, dl$$
$$- \oint_{(s_1+s_2)} (q_n)_{pr}\phi r\, dS$$
$$+ \frac{1}{2}\int_{(s_1)} (\phi_+ - \phi_- - \Delta\phi_{1,2})\left[\left(\tilde{\rho}\frac{\partial \phi}{\partial n}\right)_+ + \left(\tilde{\rho}\frac{\partial \phi}{\partial n}\right)_-\right] r\, dS$$
$$+ \frac{1}{2}\int_{(S)} (\phi_+ - \phi_-)\left[\left(\tilde{\rho}\frac{\partial \phi}{\partial n}\right)_+ + \left(\tilde{\rho}\frac{\partial \phi}{\partial n}\right)_-\right] r\, dS \qquad (II'\text{-}1)$$

From $\delta J'_{II} = 0$, one can derive the first, third and fourth rows of Equations (II-2a) and (II-2b).

(b) Sub-generalized variational principle

$$J''_{II}(\phi, \Lambda_l, \Lambda_\varphi) = \iint_{(A)} \tilde{\rho}\left\{\Lambda_l \frac{\partial \phi}{\partial l} + \frac{\Lambda_\varphi}{r}\frac{\partial \phi}{\partial \varphi}\right.$$
$$\left. + m\left[\frac{X}{\kappa} - 1 - \frac{1}{2m}(\Lambda_l^2 + (\Lambda_\varphi + \Lambda_\infty)^2)\right]\right\} r\, dA\, dl + L_{II} \qquad (II''\text{-}1)$$

where L_{II} represents the linear integration terms in J_{II};

$\bar{\rho} = X^m$

From $\delta J''_{II} = 0$, the first and second rows of (II-2a) and (II-2b) can be derived.

(c) Variational principle IV.

Using the second, third and fourth rows of Equation (II-2a) as ~~the~~ additional constraints to J_{II}, we get

$$J_{IV}(\phi) = \iint_{(A)} G_1 d\varphi dl - L_{II} \qquad (IV\text{-}1)$$

where

$$G_1 = \frac{rr}{\varepsilon}\tilde{p} = \frac{rr}{\varepsilon}\left\{1 - \frac{1}{2m}\left[\left(\frac{\partial\phi}{\partial l}\right)^2 + \left(\frac{1}{r}\frac{\partial\phi}{\partial\varphi}\right)^2 - \frac{2\Lambda_\theta}{r}\frac{\partial\phi}{\partial\varphi}\right]\right\}^{\frac{1}{m-1}}.$$

Let $\delta J_{IV} = 0$, then the first Equation in (II-2a) and Equation (II-2b) can be obtained.

Similarly, more sub-generalized variational principles can be derived from J_I and J_{II}. They will not be further discussed here.

IV. Dual extremum principle of homoentropic flow

Now we are going to prove that, under subsonic conditions, the variational principles III and IV discussed above all belong to the extremum principle. Furthermore, they form a pair of dual extremum principles.

(A) Extremum (minimum) principle V

The homoentropic subsonic flow solution of a cascade on an arbitrary stream sheet of revolution makes the general function $J_{III}(\psi)$ ~~to have a minimum~~ take an extremely small value.

Proof: It can be proven [1] that when $\delta J_{\text{~~IV~~}III} = 0$, there is

$$\delta^2 J_{III}(\psi) = \iint_{(A)} \frac{rQ_1}{r\tilde{\rho}(\tilde{a}^2 - \Lambda^2)} d\varphi dl$$

$$Q_1 = (\tilde{a}^2 - \Lambda_1^2)\left[\delta\left(\frac{\partial\psi}{\partial l}\right)\right]^2 - \frac{2\Lambda_1\Lambda_2}{r}\delta\left(\frac{\partial\psi}{\partial l}\right)\delta\left(\frac{\partial\psi}{\partial\varphi}\right) + \frac{\tilde{a}^2 - \Lambda_2^2}{r^2}\left[\delta\left(\frac{\partial\psi}{\partial\varphi}\right)\right]^2$$

It is not difficult to see that the condition to Q_1 to be positive is $\tilde{a}^2 - \Lambda^2 > 0$. Therefore, we know that at subsonic speed, the function $J_{III}(\psi)$ has a minimum.

(B) Extremum (maximum) principle VI

The homoentropic subsonic flow solution of a cascade on an arbitrary stream sheet of revolution makes the function $J_{IV}(\phi)$ to have a maximum.

The proof is similar to the above. It will not be repeated.

(C) Dual extremum principle VII

a) channels on an arbitrary stream sheet of revolution.

Under this condition the boundary sections $\overline{13}$ and $\overline{42}$ shown in Figure 1 do not exist. The distribution of ϕ along c_1 can be directly given. Therefore, the term $\int_{c_1}$ is no longer necessary in $J_{III}(\psi)$. The solutions corresponding to the extremum (expressed by using the subscript ex) can be used to write Equations (III-1) and (IV-1). They are

$$J_{III}(\psi_{ex}) = \iint_{(A)} \left\{ \frac{\tilde{p}}{\kappa} + (\Lambda^2 + \Lambda_m \Lambda_\varphi)\tilde{\rho} \right\}_{ex} \tau r d\varphi dl \qquad (\alpha)$$

$$J_{IV}(\phi_{ex}) = \iint_{(A)} \left(\frac{\tilde{p}}{\kappa} \right)_{ex} \tau r d\varphi dl + \oint_{(c_1+c_2)} (\phi q_m)_{ex} \tau dS \qquad (\beta)$$

Applying Gauss theory and also considering Equations (1a) and (1e), we can write

$$\oint_{(c_1+c_2)} (\phi q_m)_{ex} \tau dS = \oint_{(c)} (\phi \mathbf{q})_{ex} \cdot \mathbf{n} \tau dS = \iint_{(A)} \nabla \cdot (\phi \mathbf{q})_{ex} \tau r d\varphi dl$$

$$= \iint_{(A)} (\mathbf{q} \cdot \nabla \phi)_{ex} \tau r d\varphi dl = \iint_{(A)} \{\tilde{\rho}(\Lambda^2 + \Lambda_m \Lambda_\varphi)\}_{ex} \tau r d\rho dl$$

Substituting the above into Equation (β) and then comparing with Equation (α), we obtain the following important relation:

$$J_{III}(\psi_{ex}) = J_{IV}(\phi_{ex}) = J_{ex}$$

This is the dual extremum principle for channels on an

arbitrary stream sheet of revolution: Not only that, the extremum solutions ψ_{ex} and ϕ_{ex} makè the general functions J_{III} and J_{IV} have a maximum and a maximum, respectively, but also the two extrema are equal.

Generally speaking, $J_{III}(\psi) \geq J_{ex} \geq J_{IV}(\phi)$.

b) cascade on an arbitrary stream sheet of revolution.

Using treatment similar to the one described above and selecting the stream lines at stationary points in the front and rear of the blade contours as the boundaries $\overline{13}$ and $\overline{42}$, we get

$$J_{III}(\psi_{ex}) = J_{IV}(\phi_{ex}) + I_{ex} \qquad \text{(VII-1)}$$

where

$$I_{ex} = \oint_{\sigma_1} \{(A_\psi)_{ex} + i_\phi A_{ex}\} \phi_{ex} dS$$

This is then the dual exrremum principle for a cascade on an arbitrary stream sheet of revolution. Not only that, the extremum solution ψ_{ex} and ϕ_{ex} make the general functions J_{III} and J_{IV} to have a minimum and a maximum respectively, but also there exist a relation between the two extrema as described by Equation (VII-1).

V. Generalized variational principles and variational principles of non-homoentropic flow

Here the distribution of entropy $S = S(\mathbf{l}, \psi)$ is given (Figure 2(a)).

(A) Generalized variational principle (VIII)

The condition under which the general function J_V which is equivalent to the nonhomoentropic flow solution of a cascade on an arbitrary stream sheet of revolution is: $\delta J_V = 0$.

Here, Λ_l, Λ_φ, ψ, $\tilde{\rho}_0$ and $\tilde{\rho}_0$ all undergo variation independently.

$$J_V(\Lambda_l, \Lambda_\varphi, \psi, \tilde{\rho}_0, \tilde{\rho}_0) = \iint_{(A)} \left\{ \frac{\Lambda_l}{\tau r} \frac{\partial \psi}{\partial \varphi} - \left(\frac{\Lambda_\varphi + \Lambda_w}{r} \right) \frac{\partial \psi}{\partial l} - \frac{\tilde{\rho}_0}{2} (\Lambda^2 - \Lambda_w^2) - \Omega \right\} \tau r \, d\varphi \, dl$$

$$+ \oint_{(s_1)} (\Lambda_w + \Lambda_w i_\varphi) \psi \cdot dS + \oint_{(s_2)} (\Lambda + \Lambda_w i_\varphi)(\psi - [\psi(l)]_w) \cdot dS$$

$$- \frac{1}{2} \int_{(s_2')} (\Lambda_\pm + \Lambda_\mp + 2\Lambda_w i_\varphi)(\psi_\pm - \psi_\mp - \Delta\psi_{1,2}) \cdot dS$$

$$+ \frac{1}{2} \int_{(z)} (\psi_- - \psi_+)(\Lambda_+ + \Lambda_- + 2\Lambda_w i_\varphi) \cdot dS \qquad \text{(V-1)}$$

where $\Omega(\tilde{\rho}_0, \tilde{\rho}_0, \tilde{s}) = m \left\{ \frac{\tilde{\rho}_0}{\kappa} \left[1 + \Delta\tilde{s} - \ln(\tilde{\rho}_0 \tilde{\rho}_0^{-\kappa}) \right] - \tilde{\rho}_0 \right\}$

Proof: The proof is similar to the one used in the treatment of generalized variational principle I. From $\delta J_V = 0$, we can obtain the entire set of Euler equations and natural boundary conditions. With the exception that the degree of revolution equation and the homoentropic relation are replaced by (2b) and $(2c)_3$, respectively, and $\tilde{p}$ and $\tilde{\rho}$ are replaced by $\tilde{p}_0$ and $\tilde{\rho}_0$, respectively, the rest are identical to Equations (I-2a) and (I-2b). It can be seen that from the generalized variational principle VIII we can derive a nonhomoentropic flow solution of cascade which satisfies all the boundary conditions and is continuous on the artificial boundaries.

(B) Sub-generalized variational principle family

Using the method similar to the one used in Section III, we can derive another family of sub-generalized variational principle. Only one of them is listed here.

Variational principle IX

$$J_{VI}(\psi) = \iint_{(A)} \frac{\tau r}{\kappa} \exp(-m\Delta\tilde{S}) \left(1 + \frac{\Lambda_w^2}{2m} + \frac{\kappa + 1}{2} \Lambda^4 + \kappa \Lambda_w^4 \right)$$

$$\times \left[1 - \frac{1}{2m} (\Lambda^2 - \Lambda_w^2) \right]^m d\varphi \, dl + L_{III} \qquad \text{(VI-1)}$$

where L_{III} represents all the linear integration terms in J_V. From $\delta J_{VI} = 0$, we can obtain the degree of revolution Equation (2b) and the entire (natural) boundary conditions.

(C) The variational principle X expressed by the generalized flow function Θ. The condition for the following function J_{VII} which is equivalent to the nonhomoentropic flow solution of a cascade on an arbitrary stream sheet of revolution is $\delta J_{VII} = 0$.

$$J_{VII}(\Theta) = \iint_{(A)} F_1 \exp(-\Delta\bar{S}) d\varphi dl + \oint_{(\sigma_1)} \exp(-\Delta\bar{S})(\Lambda_m + \Lambda_\varphi i_\varphi)\Theta \cdot dS$$
$$+ \oint_{(\sigma_2)} \exp(-\Delta\bar{S})(\Lambda + \Lambda_\varphi i_\varphi)\{\Theta - [\Theta(l)]_m\} \cdot dS$$
$$- \frac{1}{2}\int_{(\sigma_3')} \exp(-\Delta\bar{S})(\Lambda_\perp + \Lambda_\mp + 2\Lambda_\varphi i_\varphi)(\Theta_\perp - \Theta_\mp - \Delta\Theta_{1,2}) \cdot dS$$
$$+ \frac{1}{2}\int_{(\Sigma)} \exp(-\Delta\bar{S})(\Theta_- - \Theta_+)(\Lambda_+ + \Lambda_- + 2\Lambda_\varphi i_\varphi) \cdot dS \qquad \text{(VII-1)}$$

From $\delta J_{VII} = 0$, we can get Equation (2b) and all (natural) boundary conditions [1].

VI. Regarding the actual application of the variational principle

The key here is the treatment of the various complicated boundary conditions f the cascade problem. We primarily rely on taking full advantage of the unique functions of the natural boundary conditions and the artificial boundaries. Now we are going to briefly explain the situations separately.

---

[1] In J_{VII}, let us assume that $\bar{S} = \bar{S}(l,\psi)$ is given. In practice, it is more convenient to make $s = s(l,\theta)$. But we agree that it does not undergo variation which means that $\delta(\Delta\bar{S}) = 0$. Under such conditions, the variational principle X is still valid.

In all the above variational principles, all the boundary conditions have been transformed into natural boundary conditions. Therefore, they do not have to be considered in seeking for the solution. Despite this fact, in the direct variational methods (such as Ritz method and Kantorvich method, etc.), it is still more advantagenous if the coordinate function can satisfy some of the natural boundary conditions. This would improve the accuracy of the solution. However, it is not practically possible to choose a coordinate function beforehand which will satisfy all the boundary conditions in the region when a solution is being sought. It appears that the most effective and simple method is to use the artificial boundary with high flexibility to choose the coordinate function by the region. That is to analyze the characteristics of difference in each region then first to separate them and followed by solving them. For example, in Figure 1, the characteristics of the boundary conditions between zones I, III and zone II are drastically different. Therefore, it is more proper to choose the straight line $\overline{33'}$ and $\overline{44'}$ as the artificial boundary Σ. Henceforth, in regions I and III, the coordinate function only must satisfy the periodicity requirement and in region II, it only must satisfy the blade surface conditions. In the meantime, because the linear integration terms on the Σ surface have already been added to all the variational principles, the approximate solution combined by all the regions would then automatically (although it is an approximation, yet it is the highest limit) satisfy the continuity condition on Σ.

The artificial boundaries can be used to separately process the various boundary sections with different geometric characteristics. For example, in Figure 3 $\overline{aa'}$ and $\overline{64'}$ divided the surface of the blade into sections $\overline{2a}$, $\overline{ab}$, $\overline{64}$, $\overline{3'a'}$ and $\overline{a'4'}$ with different geometric properties (arcs of various radius, sections of a parabola, etc.) and further divided region II into sub-regions II, II_2 and II_3. Therefore, the blade surface curve in each sub-

region can easily be expressed or approximated by simple analytical equations. It is then not difficult to structure the coordinate function which satisfies the boundary conditions of the blade surface. Apparently, for the simplification in the calculation of various integrations $\int_{(\Sigma)}$, the artificial boundaries should be straight lines.

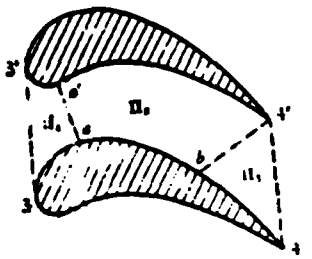

Figure 3. The method to select the artificial boundaries

Key: i) separate the regions where the characteristics of the boundary conditions are different (such as $\overline{33'}$ and $\overline{44'}$). ii) separate the boundary sections with different geometric characteristics (such as $\overline{aa'}$ and $\overline{ab}$.

In the finite element method, the boundary of each element can be used as the artificial boundary Σ. Therefore, if more undetermined parameters are added to the implantation function of each element, through the action of the $\int_{(\Sigma)}$ terms in all the general functions, it will automatically attain an optimal continuity (i.e., miscibility) on the boundary Σ of every element. The convergence and accuracy of the solution can then be assured.

In either the finite element method or the direct variational method, after an approximate function is substituted into the general function, the solution can be obtained directly using various advanced mathematical calculation methods.

VII. Conclusions

1. In the above three families of variational principles and dual extremum principles of homoentropic and nonhomoentropic flow for the direct problem of cascades and channels on an

arbitrary stream sheet of revolution were derived. The major characteristics are: a) it considered the conditions under which gas injection or suction along the surface of the blade exists in order to satisfy the requirements of the newly developed area such as boundary layer control, air film type or prespiration type of cooling, etc.; b) it takes full advantage of the special functions of the natural boundary conditions and the artificial boundaries to simplify the treatment of the boundary conditions. Thus, the practical value of these variational principles can be raised.

2. In addition to the fact that each generalized variational principle can be used to directly solve problems (through the finite element method, variational-difference method [10] or the direct variational method. The major advantage is that the distribution of flow velocity does not have to be derived from partial differentiation with respect to ψ (or ϕ, or θ) so that better accuracy can be expected. The disadvantage is that the solution is not uniquely determined. Therefore, it is more difficult to analyze convergence and error), another important feature is that a series of new sub-generalized variational principle families can be derived from them and thus providing an wide degree of freedom to choose from in its application.

3. Using the variational principles in this paper which considered the mass transfer on the surface of the blade, the condition under which suction on the blade surface exists can be treated rigorously. For the condition of gas injection on the surface of the blade, it was assumed that the H and k, etc., of the injected gas (except S) are the same as the main gas flow. If the H is different for the injected gas, a corresponding variational principle can also be derived. This will be discussed elsewhere. This method can also be used to simulate the repulsive reaction of the boundary layer of the blade surface and tail trace.

4. The various variational principles introduced in this paper are only applicable to subsonic flows and non-turbulent transonic flows (the partial supersonic section included must undergo special treatment, refer to reference [11]).

5. It can be proven that the physical meaning of the surface integration part of J_{III} and J_{VI} as well as other general functions J_1, J_1', J'', and J_V derived from the same family is the difference of kinetic energy $K(=c^2/2)$ and potential energy (internal energy) Π $(=C_v T)$ of the flowing matter in the region where the solution is obtained. Considering further the generalized enthalpy $H: \iiint_{(A)} (K - \Pi + H)\rho dV$ it can be seen that this family of the variational principles is very closely related to the Hamiltonian principle. Furthermore, the physical meaning of the surface integral part of J_{IV} and the other general functions of the same family, such as J_{II}, J_{II}' and J_{II}'' is the kinetic power of the total flowing material in the region where the solution is obtained.

6. It goes without saying that the entire variational principles discussed in this paper can be applied to treat the special case of planar flow conditions.

7. This paper considered the effect of viscosity loss in approximation by properly estimating the distribution of entropy $S(1,\psi)$. If a more perfect viscosity model is adopted, which is to add a a viscosity term $(\bar{J}_\varphi r/\lambda_1)$ to the right of Equation (2b) and then to consider it as a known quantity (it can be obtained by an iteration method), it only requires a slight modification on the nonhomoentropic variational principles discussed in the paper (by adding a surface integral term $\iint_{(A)} \frac{\bar{J}_\varphi r}{\lambda_1} \cdot \psi d\varphi dl$). Here $\bar{J}_\varphi = J_\varphi / \omega_0$ is the circumferential component of the dimensionless viscosity.

REFERNECES

1. Hu Hai Chang, Scientia Sinica, 4, 1 (1955)

2. Pang Hung Wu, Science News, 20, 9 (1975)

[3] Serrin, J., Mathematical principles of classical fluid mechanics, in Flügge (ed.), Handbuch der Physik, Vol. 8, Strömungsmechanik I, Sect. 2, Springer-Verlag (1959).

[4] Tsien, H. S. (钱学森), The eq-s of gas dynamics, in Emmons (ed.), Fundamentals of Gas Dynamics (1956).

[5] Lush, P. E. & Cherry, T. M., *Quarterly J. Mech. Appl. Math*, 9, 1 (1956).

[6] Lin, C. C. (林家翘), *Quarterly Appl. Math.*, 4 (1951).

[7] Wu, C. H. (吴仲华), NACA TN2604 (1952).

[8] Thompson, D. S., CUED/A Turbo/TR 45, Univ. Cambridge (1973).

[9] Courant, R. & Hibert, D., Methods of Mathematical Physics, Vol. I (1953).

10. Feng Kang, Applied and Computational Mathematics, 2, 4 (1965)

[11] Chau, S. T K., et al. AIAA Pap. 75—79 (1975)

CALCULATION OF UNSTARTED-CHOKED REGIME OF SUPERSONIC AND TRANSONIC COMPRESSOR CASCADES*

Cheng Jia-gang
(Institute of Mechanics, Academia Sinica)

ABSTRACT

This paper studies unstarted-choked regime of supersonic and transonic cascade, such regime is important for the starting process and offdesign regime.

A semiempirical method is given here, which allows for calculating operating incidence of this regime. Under the condition of downstream throttle, or at various the axial velocity density ratio, this method also gives useful results. Other performance parameters, such as total pressure loss, pressure ratio and flow deviation angle may be obtained simubtaneously.

In comparison with other works[1-3], the method presented here considers more variation of condition. The calculating results obtained show this method is reliable. Because this method is more simple and convenience, it may be adopted to analyse the aerodynamic performance of cascades and the influence of geometric parameters and dynamic parameters on cascade performance.

This paper studied the unstarted-choked regime of supersonic and transonic cascades. Under conditions of downstream throttle and varying axial velocity density ratio, useful results could also be obtained. In addition, other corresponding performance parameters of the cascade, such as total pressure loss, pressure ratio and flow deviation angle can also be obtained. In comparison with other works reported by foreign researchers, this method may be used to take more variations of condition into consideration. The results of our calculation, after the comparison, indicated that this method is reliable. Since this method is relatively simple, it may be used to analyze the performance characteristics of the cascade. Furthermore, it may be used to analyze the performance characteristics of the cascade under conditions that geometric and dynamic parameters vary.

*Received on April 3, 1978.

SYMBOLS

M Mach number

K experimental constant

w gas flow velocity

a speed of sound

β gas flow angle (in reference to the axis of the blade)

b thickness of the flow layer

$p(p^o)$ static pressure of the gas flow (total pressure)

ρ density of the gas flow

L hydrodynamic factor of the cascade

V Reynolds factor of the cascade

U Mach factor of the cascade

σ density of the cascade

β_s installation angle

ϕ deviation angle

R_e arc length Reynolds number

J efficiency correction factor

τ_2 thickness at the rear end of the blade

Q axial ~~velocity~~ density ratio

S_t/t compression ratio at the throat

A_2^*/t downstream throttle ratio

γ specific heat ratio

q(M) critical compression ratio

η_o subsonic cascade varying efficiency

c arc length

t nodal distance

$\bar{\omega}$ coefficient of total pressure loss

p_2/p_1 cascade pressure increase ratio

$\Delta\beta=\beta_1-\beta_2$ gas flow deviation angle

T temperature of the gas flow

Q/Q_{max} flux ratio

Subscripts:

1. Flow far in front of the cascade

2. Flow way downstream from the cascade

No subscript:

Flow behind the shock wave in the duct

There are three types of inlet flow patterns for supersonic cascades: unstarted flow pattern (or mixed type), started flow pattern (supersonic type) and saturated flow type (supersonic axial velocity type). The characteristic of the first type is that there is a quasi-normal shock which is detached from the object in the inlet region. The second flow pattern is the appearance of an oblique shock wave which is attached to the object in the inlet region. It is supersonic in the duct and in a started condition. The back pressure from downstream cannot influence the flow pattern of the inlet area. The saturated flow pattern appears when the Mach number of the incoming flow is even higher (for example $M_1 > 2$). At this time, the velocity component along the axis of the cascade becomes supersonic. The shock wave and Mach wave are limited to the inside of the duct of the cascade. During the starting process of the cascade, when M_1 varies from lower to higher number, these three types of flow pattern can appear in sequence. The superiority of the saturated flow pattern is only limited to the supersonic aerospace vehicles which has not been studied extensively at this moment.

In a compressor with shock wave inside the rotor, as soon as after the entire blade height reaches supersonic condition, the characteristic will appear to be very steep as shown in Figure 1. The vertical section represents the unstarted choked flow pattern. Its upper limit of Mach number (=1.2-1 5) is determined by the area of the throat region and the dullness of the front fringe. The curved section represents the unstarted unchoked flow pattern. Its study will assist in the prediction of loss of velocity. After M_1 has exceeded the upper limit, the cascade then moves into the started working condition. The characteristic steepness is created by the sole attack angle (or the periodicity of the flow limits the flux). Apparent in the characteristics of variation of working conditions in a compressor, there are many situations (especially under low revolution speed and high back pressure conditions) which

belong to the unstarted choked flow pattern.

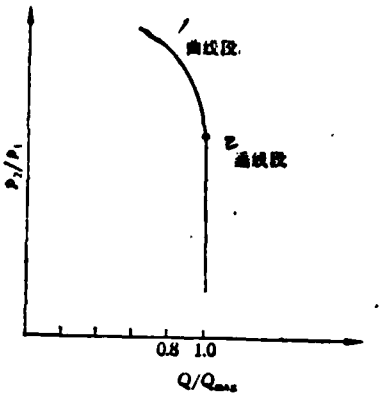

Figure 1. The characteristics of a supersonic compressor

Key: 1--curved section
2--vertical section

Presently, more working conditions are designed to use the started flow pattern. However, the unstarted choked flow pattern has also been used to design the working condition of the first order stator (to prevent the propagation of noise forward). In addition, it was proved in [1] that the use of the unstarted intense oblique shock wave series design for rotors is more superior than using the multiple arc cascade at high pressure ratios. This paper studied the unstarted choked working condition of supersonic cascades. In the judgment of the operating attack angle of this type of flow pattern, there have been many researchers abroad studying this problem using semi-empirical methods [2-5]. This paper provided a relatively simple method to calculate the operating attack angle of the choked flow pattern encountered during the starting process or the variation of working conditions. It also considered the effect of the back pressure from downstream and the axial density ratio on the operating attack angle.

In order to calculate the attack angle β_1, it is necessary to study other characteristics of this flow pattern, such as loss, pressure ratio, etc. Owing to the complexity of the problem very often people would adopt various postulated flow model and/or semi-empirical calculation methods which ignore the position and shape of the shock wave as well as its connection with the characteristics of the boundary layer in order to study the main factors influencing

the loss. They have provided very valuable information [6,7] in the areas of research, design and experimentation. This paper referred to the treatment used in [7] to offer a simple model of cascade loss to calculate other properties of the cascade.

I. ANALYSIS

Because the characteristic curve of supersonic and transonic compressors is steep, it is approximately an equi-mass flow rate line, the correct estimation of its operating attack angle β_1 is very important. A 1° difference in β_1 can result to a 5% difference in flux. One of the reasons why the early stage failure in the development of the supersonic compressor is the lack of accuracy in calculating the flow angle. It was impossible to design the blade profile with small loss. Thus, the efficiency was very low.

The flow of a planar cascade is basically two-dimensional. When M_1 of the incoming flow is higher, shock is created. The starting shock wave originates as a supersonic bag on the back of the blade and begins to develop into a quasi-normal shock wave across the entire duct with increasing M_1. Based on the suggestion by Ferri [2], the intensity of the shock wave in the duct is higher than the heat wave. Therefore, in the one-dimensional analysis, it only considers the proper making of assumptions of intensity and position with respect to the shock wave in the duct (it is also called the starting shock wave in the starting process). It does not care about the actual shape of the shock wave. The heat wave is neglected completely. Many authors assumed that the unstarted flow pattern is the normal shock wave inlet model. Therefore, the gas flow is not deflected after the shock wave and the intensity of the wave is only affected by the incoming flow M_1 which is realtively crude. Actually, in addition to the effect of M_1, the shock wave in the duct is also influenced by many factors,

such as the reverse pressure. Furthermore, the flow behind the wave is deflected.

For simplicity, let us assume the flow is one-dimensional and the shock wave in the duct deflects the incoming flow from β_1 direction to β direction. The proper selection of the β value can improve the accuracy of the analysis. Apparently, the choice of β is affecting the outcome of the calculation significantly. If we choose $\beta = \beta_1$, it is then equivalent to the normal shock wave case. Chauvin [4] suggested that the average direction of the duct at the inlet of the cascade be β. However, Fabri [3] recommended the direction of zero rising force of the cascade to be β. In this paper, however, we used the geometric average direction of the gas flow directions at the inlet and the outlet as the direction of gas flow after the shock wave in the duct.

For compressible viscous gases, average geometric direction and zero rising force direction are different. Using the former to substitute the latter makes it much simpler in the treatment. Only that the gas flow direction at the outlet of the cascade β_2 must still be known. In the position-flow calculation of a finite thickness rounded rear fringe cascade, β_2 and the ring quantity are in principle uncertain. This is also the common drawback of all position flow calculation methods. Theoretically, we can use the rear pressure region to replace the rear stationary print to perform a calculation to compensate for viscosity to solve the problem. However, it is still hard to solve the flow in separated regions. Therefore, many research work switched to the use of comprehensive data obtained from cascade experiments to seek for solution. They performed statistical analysis on the experimental results obtained from various types of wind tunnel and various subsonic cascade wind tunnels with different geometric parameters and dynamic parameters and found that r and $\cos \beta_1 / \cos \beta_2$ has a dependence relationship close to that of a hyperbolic curve [8] (Figure 2). In the same figure some experimental data of supersonic cascade and supersonic

rotor are also plotted. Therefore, in this paper we assume that $Q \cos \beta_1 / \cos \beta_2 = K$ is the supplementary equation for the gas flow angle at the exit. The value of K should vary depending on the geometric and dynamic parameters of the cascade. It is most appropriate either to determine it experimentally or to choose its value based on lots of statistical data. As for the data gathered in Figure 2, it is more suitable to let K = 0.75-0.8. The physical meaning of K can be considered as the flow density ratio at the inlet and the outlet. It is apparent that in a compressor cascade the variation of p_2/ρ_1 and w_2/w_1 has a mutually weakening affect. Their products are not very sensitive to the variations of other parameters.

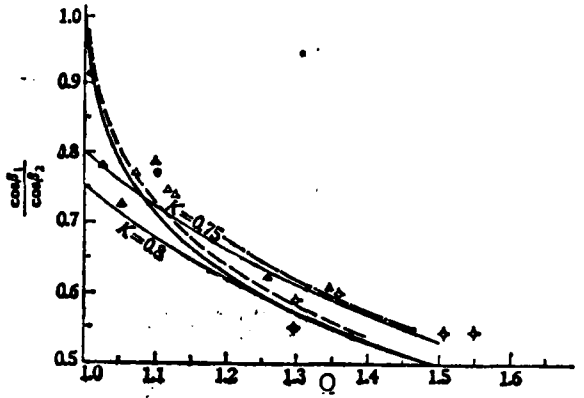

Figure 2. Relation between measured flow angle of compressor cascade and Q.

—	[11]	NACA065	—	$M_1 \leqslant 0.8$
—	[8]	C4	$\delta = 5$	$M_1 \ll 1$
—·—	[8]	C4	$\delta = 2$	$M_1 \ll 1$
◇	[7]	BTE	$\delta = 3$	$M_1 = 1.56$
●	[10]	MCA	$\delta \approx 2$	$M_1 = 1.4$
✱	[4]	Rotor	—	$M_1 = 1.2$—1.54

In [9], some crude non-compressible analysis was given to this hyperbolic relationship obtained based on experimental statistics. That paper assumed that separation occurred at a certain point on the back of the blade. The local diffusion factor is $D_{sep} = W_{sep}/W_{max}$. Because the separation region remains to be isobaric, that is D_{sep} is invariant, the velocity on the outside of the separation region is $W_2 = W_{sep}$. It was further assumed that the main flow which did not suffer velocity loss could still be deflected to the nominal β_2^* angle direction, then we get:

$$\sigma = \frac{w_1 \cos\beta_1^*}{w_1 \cos\beta_1} = \left(\frac{w_{sep}}{w_{max}}\right)\left(\frac{w_{max}}{w_1}\right)\frac{\cos\beta_1^*}{\cos\beta_1}$$

$$\sigma \frac{\cos\beta_1}{\cos\beta_2} \approx \sigma \frac{\cos\beta_1}{\cos\beta_1^*} = D_{sep}\left(\frac{w_{max}}{w_1}\right)$$

For a given cascade, w_{max}/w_1 is approximately invariant and D_{sep} is a constant. Therefore, the right hand side of the above equation is approximately a constant.

Because the pressure increase of a supersonic and transonic cascade is relatively larger, the effect of compressibility on the average geometric direction should be considered. The subscripts u and a are used to represent the facial and axial components of the gas flow velocity in the cascade, respectively. Then after dividing

$$w_a = (w_{1u} + w_{2u})/2, \quad w_a = w_{1a}[1 + (w_{2u}/w_{1a})]/2$$

$$w_{2u}/w_{1a} = \sigma\rho_1/\rho_2, \quad \text{we get}$$

$$tg\beta = \left(tg\beta_1 + \sigma\frac{\rho_1}{\rho_2}tg\beta_2\right)\Big/\left(1 + \sigma\frac{\rho_1}{\rho_2}\right)$$

when $\sigma = 1$, and $\rho_1/\rho_2 = 1$, this equation is reduced to $tg\beta_1 = (tg\beta_1 + tg\beta_2)/2$. It is obvious that in order to solve for β_1, we must consider other characteristics of the cascade, such as the cascade density, etc. To calculate the cascade loss, it is not sufficient to calculate the shock wave in the duct term alone. The model adopted by this paper, in general, was that the unstarted supersonic

shock wave in the duct deflected the incoming flow to the average geometric direction of the cascade and stowed it down to subsonic. The flow behind the wave traveled through the subsequent subsonic compressors in a one-dimensional flow manner. The optimal variational efficiency of compression η_o is related to the hydrodynamic factor of the cascade L, Reynolds factor V and Mach number factor U based on the dimensional analysis given in [10]. Other losses not accounted for, such as shock wave boundary layer interference, tail trace mixing, etc., are represented by the efficiency correction factor f obtained based on the statistical treatment of experimental data. In the situation that experimental data are lacking, the results listed in [7] will be used temporarily.

Through the above analysis, we can briefly describe the assumptions made in our calculation as follows:

i. The flow passing through the cascade is basically one-dimensional. With no flow restriction, the throat is at the same state.

ii. Neglecting the heat wave, we assume that the shock wave in the duct deflects the incoming flow to the average geometric direction of the gas flow at the inlet and outlet.

iii. There exists the experimental statistical rule $Q\cos\beta_1/\cos\beta_2 = K$ and K is determined experimentally.

IV. The subsonic cascade loss behind the shock wave in the duct is mainly due to the compression loss η_o and separation loss f.

II. DERIVATION OF EQUATIONS

Let M, β, p, p^o and b represent the Mach number, gas flow angle, static pressure, total pressure and thickness of the flow layer of the gas flow behind the shock wave in the duct respectively. The subscripts 1. and 2. respectively represent the direction of

gas flow in the front and back of the cascade. Using the flow parameters in the front and behind the shock wave in the duct, we can write the momentum conservation equation in the β direction (through continuous equation transformation)

$$p + \rho w^2 = p_1 \frac{b_1}{b} + \rho w w_1 \cos(\beta_1 - \beta) \tag{1}$$

Using the state equation and the sound velocity expression, we get

$$\frac{M \cos\beta}{M_1 \cos\beta_1} = \frac{a}{a_1}(1 + \gamma M^2) - \gamma M M_1 \cos(\beta_1 - \beta) \tag{2}$$

Equation (2) can be used to calculate the operating attack angle β_1 of the unstarted choked flow pattern. To carry out the calculation, it is also necessary to be supplemented by additional relations. Let us assume that iii can be used. In addition, because the region behind the wave is the upper subsonic region, the throat of the cascade S_t (or the effective throat created due to viscosity) is usually in a critical state. Therefore, the following equation can be used:

$$\frac{S_t}{t \cos\beta} = M\left(\frac{\gamma + 1}{2 + (\gamma - 1)M^2}\right)^{\frac{\gamma+1}{2(\gamma-1)}} = q(M) \tag{3}$$

q(M) is defined as the critical contraction ratio. Under the condition of downstream throttle, the throat is located at the throttle. In calculation the extent of opening of the throttle A_2^* should replace S_t.

Then from assumption ii, the flow direction β behind the shock wave in the duct is the average geometric direction of the cascade, it is obtained under the equi-Ω condition that:

$$\operatorname{tg}\beta = \left(\operatorname{tg}\beta_1 + \Omega \frac{\rho_1}{\rho_2} \operatorname{tg}\beta_2\right) \Big/ \left(1 + \Omega \frac{\rho_1}{\rho_2}\right) \tag{4}$$

Using Equations (2)-(4), we can obtain the four unknowns $\beta_1(M_1)$, $M(M_1)$, $\beta(M_1)$ and $\beta_2(M_1)$ with given Ω and S_t/t (or $A_2^*(t)$ where $\beta_1(M_1)$ is the operating attack angle which we want to determine. During the process ρ_1/ρ_2 is set ahead of time and it is checked against other parameters of the cascade when the solution is obtained.

Therefore, it is an iterative process. After the flow parameters behind and in front of the shock wave in the duct, the static pressure use and the total pressure recovery coefficient of the shock wave in the duct can be directly obtained from the continuous equation

$$\frac{p}{p_1} = \frac{\rho T}{\rho_1 T_1} = \frac{b_1 w_1 \cos\beta_1}{b w \cos\beta} \frac{a^2}{a_1^2} = \frac{b_1}{b} \frac{M_1 \cos\beta_1}{M \cos\beta} \left[\frac{1 + (\gamma-1)M_1^2/2}{1 + (\gamma-1)M^2/2}\right]^{\frac{1}{2}} \tag{5}$$

Let us take $b = (b_1+b_2)/2$ in approximation and then we get

$$\frac{p^0}{p_1^0} = \frac{2Q}{Q+1} \frac{M_1 \cos\beta_1}{M \cos\beta} \left[\frac{1 + (\gamma-1)M^2/2}{1 + (\gamma-1)M_1^2/2}\right]^{\frac{\gamma+1}{2(\gamma-1)}} \tag{6}$$

For the gas flow behind the shock wave in the duct in the subsonic cascade, its optimal compression efficiency can be analyzed using the results of dimensional analysis given in [10].

$$\left(\frac{1-\eta_0}{0.14\eta_0}\right)^2 = \frac{L^{0.75}}{V^{1.25}U^{0.225}} \tag{7}$$

η_o is the varying efficiency. The three parameters on the right hand side of Equation (7) are

$$L = \frac{\sigma}{\cos\beta_s \cos^2\phi}, \quad V = \log_{10}\left[\frac{\mathrm{Re}}{\sigma^{0.25}\cos\phi}\right], \quad U = \left[1 + \frac{\gamma-1}{2}M^2\right] \tag{8}$$

where $\sigma = c/t$ is the density, β_s is the installation angle, ϕ is the middle arc angle and Re is the Reynolds number of the arc length.

In order to consider losses due to shock wave in the duct and boundary layer interference, etc., a correction factor f is introduced to the relation between η_o and the total pressure recovery coefficient:

$$f\eta_0 = \left[\left(1 + \frac{\gamma-1}{2}M^2\right)\left(\frac{p_2^0}{p^0}\right)^{\frac{\gamma-1}{\gamma}} - 1\right] \Big/ \left(\frac{\gamma-1}{2}M^2\right) \tag{9}$$

Reference [7] gathered lots of data and obtained the following using a linear relationship

$$f = 1 + \frac{4}{5}\frac{\delta}{\delta + \tau_3}\left[\frac{1}{M_1^2} - \frac{1}{M_1}\right] \tag{10}$$

τ_2 is the thickness of the rear fringe, $t/(t+\tau_2)$ can be used to represent the expansion area ratio whose effect on the loss is reasonable. Under the condition that a profound study is not carried out, we are going to temporarily use this correction factor expression here.

Using Equations (6)-(10), we can write the total pressure recovery coefficient of the supersonic cascade

$$\frac{p_2^0}{p_1^0} = \left[\frac{1+(\gamma-1)\eta_0 M^2/2}{1+(\gamma-1)M^2/2}\right]^{\frac{\gamma}{\gamma-1}} \left\{\frac{2\Omega}{\Omega+1}\frac{M_1\cos\beta_1}{M\cos\beta}\left(\frac{1+(\gamma-1)M^2/2}{1+(\gamma-1)M_1^2/2}\right)^{\frac{\gamma+1}{2(\gamma-1)}}\right\} \tag{11}$$

Other properties of the cascade are

$$\sigma = \left(1-\frac{p_2^0}{p_1^0}\right)\Big/\left[1-\left(1+\frac{\gamma-1}{2}M_1^2\right)^{\frac{\gamma-1}{\gamma}}\right] \tag{12}$$

$$\frac{p_2}{p_1} = \frac{p_2^0}{p_1^0}\left[\frac{1+(\gamma-1)M_1^2/2}{1+(\gamma-1)M_2^2/2}\right]^{\frac{\gamma}{\gamma-1}} \tag{13}$$

$$\frac{\rho_2}{\rho_1} = \frac{p_2^0}{p_1^0}\left[\frac{1+(\gamma-1)M_1^2/2}{1+(\gamma-1)M_2^2/2}\right]^{\frac{1}{\gamma-1}} \tag{14}$$

When using Equations (13),(14), we must know M_2. It has been known that $[\Omega\cos\beta_1/\cos\beta_2] = [\rho_2 w_2/\rho_1 w_1] = K$. and $[\rho_2 w_2/\rho_1 w_1] = p_2^0 q(M_2)/p_1^0 q(M_1)$. Combining the two equations, we can get

$$q(M_2) = Kq(M_1)\Big/\left(\frac{p_2^0}{p_1^0}\right) \tag{15}$$

q(M) is called the flow density function or the critical contraction ratio, which is defined as

$$q(M) = \frac{\rho w}{\rho^* a^*} = \frac{A^*}{A} = M\left(\frac{\gamma+1}{2+(\gamma-1)M^2}\right)^{\frac{\gamma+1}{2(\gamma-1)}} \tag{16}$$

Here parameters carrying the * symbol are called critical parameters.

The value of ρ_2/ρ_1 obtained from Equation (14) should be consistent with the assumed value in equation (2)-(4). Otherwise, we must correct the assumed value and begin the iteration process.

III. SOLUTION PROCEDURE AND RESULTS OF CALCULATION

It is not complicated to solve the above equations. Equations (2) - (4) may be used individually to find β_1, and correspondingly to obtain the gas flow parameters behind the channel shock wave. In obtaining the solution, one should first assume a value for the ratio ρ_2/ρ_1 of the densities in front of and behind the blading. It is best in actual procedures of solving the equation to assume β_1 first, and then to find the root of M_1 from Equation (4). There are two roots, corresponding to the supersonic solution and the subsonic solution. Thus there is one β_1 corresponding to two M_1. Equations (5)-(16) are used to compute the other properties of the blading and to check the assumed value of ρ_2/ρ_1. This is an iteration procedure. When the necessary accuracy is reached, the angle of attack and other properties of the corresponding supersonic and trans-sonic blading may then be obtained.

The results obtained by using this method on the triangular blading in Figure 3 are shown in Figures 4-7. In Figure 3, the shape of the blading and necessary data are given. This is also the blading calculated by Fabri. Since our model is basically one-dimensional, its results may be borrowed for blading with similar geometric and dynamic parameters.

Since experimental data are lacking, we take K = 0.8 from Figure 2. The results of this paper are computed with K=0.8. If we take K = 0.75, the curve for the angle of attack will lie above the curve for K = 0.8 (not shown).

The calculated results for 3 types of one-dimensional models of Fabri are plotted in Figure 4. Compared to results of our paper, the trends of the variation agree and the

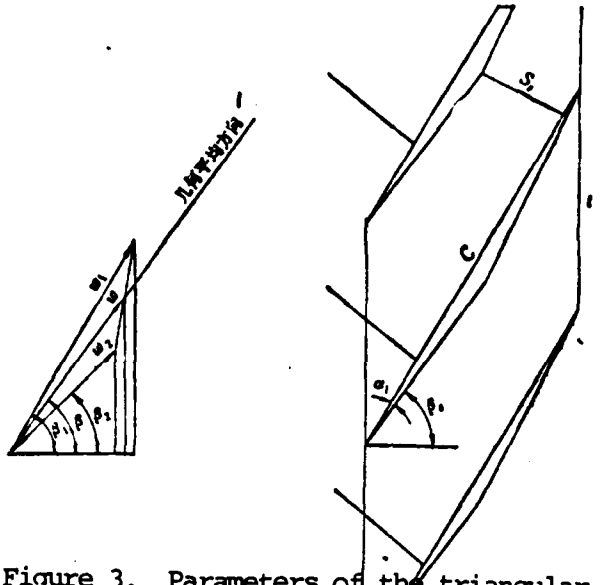

Figure 3. Parameters of the triangular cascade and the velocity triangle.

$t = 32.4$mm $c = 60$mm $S_t = 14.1$mm

$\alpha_1 = 4°$ $\beta_1 = 60°$

320

Key: 1--average geometric direction

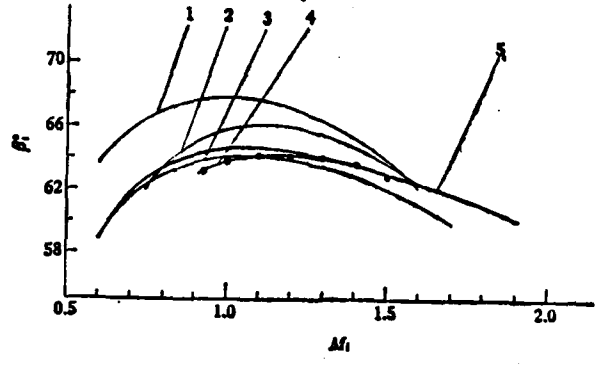

Figure 4. Calculation of the operating attack angle of unstarted choked regime of a triangular cascade (K = 0.8)

1--shock wave formed in the average direction of the end of the duct (recommended by Chauvin); 2--shock wave deflection (recommended by Fabri); 3--formation of normal shock wave in the direction of the incoming flow; 4--experimental data (ONERA special permission [4]; 5--calculated results in this work (Q = 1.0)

difference in the value of the operating attack angle is not large. Because we did not find any experimental data on the calculation of triangular cascade, an experimental curve was also included as a reference in the figure which was allowed to be published with the special permission of ONERA. Figure 5 reflected the effect of the axial flow density ratio Q on the operating attack angle of the unstarted choked cascade. The effect of Q has not been considered by other methods. $Q > 1$ corresponds to the increasing contraction ratio at the throat of the cascade. At this time, it requires a larger variation for β_1 to make the starting progress along the choked curve. Figure 6 gave the effect of throttle behind the cascade and made a comparison with the result obtained from a two dimensional model in [5]. The trend of variation appears to be consistent. The attack angles only differ by 2-3°. Part of the reason may be attributed to the fact that the two calculations were made based on different cascades. The two-dimensional model in [5] cannot calculate the transonic region enar $M_1 = 1$. Therefore, it is connected by a dotted line in the figure. Figure 7 plotted other properties of the unstarted choked cascade, including the total pressure loss coefficient $\bar{\omega}$, static pressure rise p_2/p_1 and deflection angle $\Delta\beta$. Their variation trend with M_1 and effects on Q more or less reflected the actual situation [11,12].

The calculation of loss due to shock wave in the duct indicated that the total pressure loss is larger than the total pressure loss caused by the incoming flow M_1 and the normal shock wave. This is due to that the actual wave series at the inlet of the cascade should contain an infinite number of wavefronts ahead of the quasi-normal shock wave in the duct produced by the "preceding blades", [12].

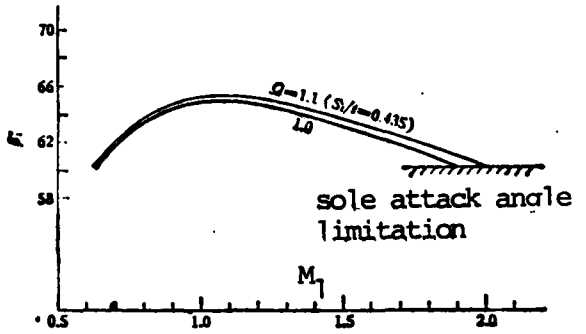

FIGURE 5. The calculation of the operating attack angle of unstarted choked regime of supersonic and transonic compressor cascades (varying axial velocity density ratio) ~~(K≤0.8)~~ (K=0.8).

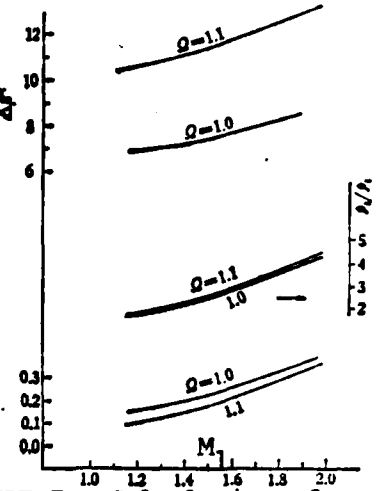

FIGURE 7. Calculation of properties of the unstarted choked regime of supersonic and transonic cascades (varying axial velocity dens. ratio)

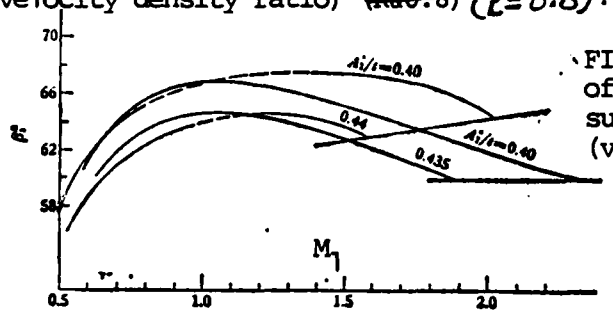

FIGURE 6. Calculation of unstarted choked regime of supersonic and transonic planar cascades (varing throttle ratio). Calculated results in [5]. Calculated results in this work.

IV. CONCLUSIONS

This paper provided a relatively simple calculation method which is capable of calculating the operating attack angle and the corresponding characteristics of the cascade of unstarted choked regime of the supersonic and transonic cascades. The results were compared to those reported in [3]-[5] which indicated that the method introduced in this paper is valuable. It can also consider the effect of downstream throttle and axial velocity density ratio variation. Q has a very important effect on the characteristics of the cascade and this is well known. More calculation should be

carried out on these supersonic and transonic cascades with some experimental results in order to further improve and verify this method. It is more important to investigate the selection of the value of K.

During the derivation and calculation stages of this paper, instructions have been given by Professor Wu Chung Haw.

REFERENCES

[1] Huffman, G. D. & Tramm, P. C., *J. of Aircraft*, 11 (1974), 682—689.
[2] Erwin, J. R. & Ferri, A., The Supersonic Compressor, Section G, in W. R. Hawthorne (ed.), Aerodynamics of Turbines and Compressors, Vol. X of the 12-Volume Work, High Speed Aerodynamics and Jet Propulsion, Princeton University Press (1964), 368—432.
[3] Fabri, J. (ONERA), Mass flow Limitation in Supersonic Compressors, AGARD Lecture Series 39(AD710893).
[4] Chauvin, J., et al. (VKI), Flow in cascades with a transonic regime to be published, in L. S. Dzung (ed.), Flow Research on Blading (1970).
[5] Lichtfuss, H. J. & Starken, H. (DLR), Supersonic cascade flow, to be published in D. Küchemann, et al. (ed.), Progress in Aerospace Sciences, Vol. 15 (1974).
[6] Boxer, B., A Method for predicting the performance of high reaction supersonic compressor blade sections, AIAA 69—522.
[7] Wells, W. R., Supersonic compressor losses, AD761107, p.p. 234—246.
[8] Celikovsky, K., One dimensional analysis of the properties of the elementary supersonic axial flow compressor cascade, 76-018-2/4.
[9] Horlock, J. H. & Mech, E., Some recent research in turbomachinery, Proc. Inst. Mech. Engrs., 182 (26) (1968), 571—594.
[10] Losey, D. & Tabakoff, W., *J. of Aircraft*, 4, 2 (1967), 133—136.
[11] Schlichting, H. & Stark, U., Influence of the ratio of axial velocities upstream and downstream of the cascade on the aerodynamic coefficient of a plane compressor cascade, AEC, K Trans—70.

THE NUMERICAL COMPUTATION FOR DIFFRACTION AND REFLECTION OF A TRAVELING SHOCK WAVE FROM AN OPEN END OF A SHOCK-TUBE

Du Xun, Wei Zhong-lei, Li Wen-xuan, Wang Jia-jun

ABSTRACT

When a shock wave travells into atmosphere from an open end of a shock-tube, an over-pressure field is induced and wave diagrams of shock diffraction and reflection form immediately. In general, one can always compute the outflow problem by solving the unsteady two-dimensional gasdynamic equations. Computing this problem numerically, the authors take advantage of Eulerian coordinates, fictitious viscosity and finite difference method. In order to decide the boundary conditions for computation at the end of tube, first we find out analytical solution for the unsteady one-dimensional flow in a shock-tube, and then the variations of the velocity, pressure and density of the flow at the open end of the tube with time. The present numerical results are in agreement with the experiments.

The wave diagram and the over-pressured field induced by traveling shockwave from the open end of a shock-tube can be simplified into a two-dimensional diffraction and reflection problem of an unsteady shockwave. This set of gas dynamic equations is non-linear. The solution would show interruptions with time. Even if the initial value is a continuous function, there may be interruptions in the solution. This causes some difficulty. In this paper, the authors adopted Eulerian coordinates, artificial viscosity and a finite difference method to obtain the solution. In order to write the boundary conditions at the end of the tube, an analytical solution to a one-dimensional gas flow in a tube was first found. From this solution, the time varying curves of the velocity, pressure and density at the end of the tube can be computed. The calculated results were compared with the experimental ones, and the two were found to be consistent. We have investigated

the wave forms of the diffraction of the shockwave traveling from the end of the tube, the slanted reflection of the shockwave from the ground, the normal reflection of the shockwave from a perpendicular barrier, the slope climbing process of the shockwave and the formation and development of the rotating ring at the end of the tube using a shadow tracing method. Simultaneously, the overpressure field distribution outside the end of the tube induced by the series of shockwaves was also measured. Numerical computations were also carriedout in this paper for the diffraction and reflection flow fields after the shockwave traveled through the end of the tube.

I. Gas dynamic equations

Neglecting viscosity and thermal conductivity and with constant specific heat, the set of dimensionless gas dynamic equations for unsteady gas flow is:

$$\frac{\partial f}{\partial t} + \frac{\partial F}{\partial x} + \frac{\partial G}{\partial y} = -\psi \qquad (1)$$

$$f = \begin{pmatrix} \rho \\ \rho u \\ \rho v \\ \rho q^2 + \frac{25}{7} p \end{pmatrix} \qquad (2) \qquad F = \begin{pmatrix} \rho u \\ \frac{5}{7} p + \rho u^2 \\ \rho u v \\ (\rho q^2 + 5p) u \end{pmatrix} \qquad (3)$$

$$G = \begin{pmatrix} \rho v \\ \rho u v \\ \frac{5}{7} p + \rho v^2 \\ (\rho q^2 + 5p) v \end{pmatrix} \qquad (4) \qquad \psi = \frac{\nu v}{y} \begin{pmatrix} \rho \\ \rho u \\ \rho v \\ \rho q^2 + 5p \end{pmatrix} \qquad (5)$$

where $\rho = \bar{\rho}/\rho_0$, $p = \bar{p}/p_0$, $v = \bar{v}/a_0$, $u = \bar{u}/a_0$, $x = \bar{x}/D$, $y = \bar{y}/D$, $t = \bar{t}/(D/a_0)$, $q^2 = u^2 + v^2$, , specific heat of air $\kappa = 1.4$, ρ_0 and p_0 are the density and pressure at standard atmospheric conditions, D is the characteristic diameter of the shock-tube. The symbols with a bar on top represent quantities with dimensions. For planar problems $\nu = 0$; for symmetric axial problems, $\nu = 1$.

II. Boundary conditions and initial conditions

1. Boundary conditions on solid walls and symmetrical axes

As shown in Figure 1, the boundary conditions are: On a horizontal solid wall $v = 0$; on a vertical solid wall $u = 0$; on a slant wall (slant wall angle is ψ)

$$-u\sin\psi + v\cos\psi = 0 \tag{6}$$

For symmetrical gas flow about an axis, on the symmetric axis $y = 0$

$$v = \frac{\partial \rho}{\partial v} = \frac{\partial e}{\partial y} = \frac{\partial u}{\partial y} = 0 \tag{7}$$

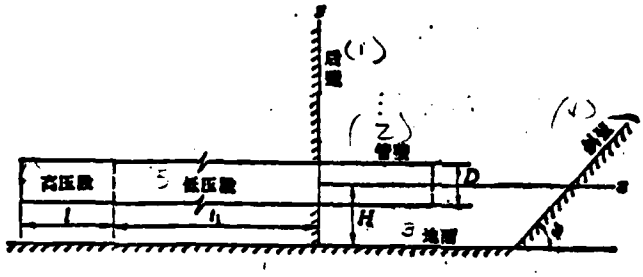

Figure 1.

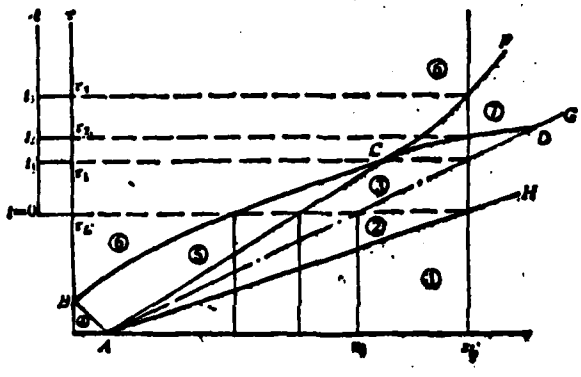

Figure 2

Key: to Figure 1.

Key: 1--rear wall; 2--tube wall; 3--ground; 4--slant wall; 5--low pressure; 6--high pressure; stage.

stage

2. Boundary conditions at the end of the tube

As shown in Figure 2, analytical solutions can all be found in regions (1)-(7) for the gas flow in a one-dimensional shock-tube. At the end of the tube, the flow is supersonic. Therefore, the velocity, pressure, density at the end of the tube are completely determined by the one-dimensional flow inside the shock-tube. Region (1) is an undisturbed region: $p_1 = \rho_1 = 1$, $u_1 = 0$. Region (2) is the shockwave compression region:

$$p_2 = (7\theta^2 - 1)/6 \tag{8}$$

$$u_2 = 5[\theta - (1/\theta)]/6 \tag{9}$$

$$\rho_2 = 6\theta^2/(5 + \theta^2) \tag{10}$$

θ is the dimensionless shockwave moving velocity. It is defined as $\theta = \bar{\theta}/a_0$. Region (3) is the uniform region behind the contact interruption plane:

$$p_3 = p_2, \quad u_3 = u_2 \tag{11}$$

$$\rho_3 = p_2/a_3^2 \tag{12}$$

$$a_3 = 1 - (u_2/5) \tag{13}$$

Here $a = \bar{a}/a_0$; therefore, $a = \sqrt{p/\rho}$. Region (4) is the high pressure region of the shock-tube. In the computations, let $p_4 = \rho_4 = 10$, and $u_4 = 0$. In addition, there is a relation between p_4 and p_2:

$$p_4 = p_2\left(1 - \frac{p_2 - 1}{\sqrt{42p_2 + 7}}\right)^{-7} \tag{14}$$

If the value of p_4 is given for a flow in the shock-tube, the shockwave intensity p_2 and θ_2 produced can be calculated.

In regions (5), (6) and (7) $p/\rho^{1.4} = p_4^{-2/5} = \text{constant}$. Using $p = \rho_a^2$ to substitute into it, we get

$$\rho = \rho_4 a^5, \quad p = p_4 a^7 \tag{15}$$

Therefore, for the solutions for the non-uniform regions (5), (6) and (7), we only have to write the expressions for a and u.

Region (5) is the central dilute wave region. Its solution is

$$a + \frac{u}{5} = 1, \quad u = \frac{5}{6}\left(1 + \frac{x-1}{\tau}\right) \tag{16}$$

where $x = \bar{x}/l$, $\tau = t/(l/a_0)$, l is the length of the high pressure section; τ is the time period from the membrane breaking moment of the shock-tube.

Region (6) is the non-uniform dilute wave interference region. Its solution is (define $\xi = \mu/5$)

$$\tau = \frac{3\xi^4 - 6(a^2+1)\xi^2 + 3a^4 + 2a^2 + 3}{8a^3} \tag{17}$$

$$x = \xi\left(5\tau + \frac{\xi^2 - 3a^2 - 1}{2a^3}\right) \tag{18}$$

Region (7) is the simple wave region. Its solution is

$$a - (u/5) = a_3 - (u_3/5) = c \tag{19}$$

i.e., $\xi = a-c$ and c is a constant. Substituting into Equations (17) and (18), we obtain the equation of the boundary life CF of region (6) and region (7).

$$\tau = \bar{\tau}(a) = \frac{4(3c^2-1)a^2 - 12c(c^2-1)a + 3(c^2-1)^2}{8a^3} \tag{20}$$

$$x = \bar{x}(a) = (a-c)\left[5\bar{\tau}(a) - \frac{2a^2 + 2ca + 1 - c^2}{2a^3}\right] \tag{21}$$

Because the first family characteristic curve is a straight line, therefore

$$x = \bar{x}(a) + (u+a)(\tau - \bar{\tau}(a)) \tag{22}$$

The solution for region (7) can be obtained from the simultaneous Equations (19)-(22).

From Equation (16) we get $\xi = u/5 = 1-a$. Substituting it into Equations (17) and (18), we obtain the equation $x = 1 + 5\tau - 6\tau^{2/3}$ for the boundary line BC between region (6) and region (5). The coordinates of point C can also be obtained

$$\tau_c = \frac{1}{a_1^3}, \quad x_c = 1 + \frac{5}{a_1^3} - \frac{6}{a_1^3} \tag{23}$$

The boundary line CD between region (3) and region (7) is a characteristic line. Its equation is

$$x - x_c = (u_3 + a_3)(\tau - \tau_c) = (u_1 + a_1)(\tau - \tau_c) \tag{24}$$

The equation of the contact interruption plane AD is

$$x = 1 + u_1\tau \tag{25}$$

Solving Equations (24) and (25) simultaneously, we get the coordinates for point D:

$$\tau_D = \frac{2}{a_1^3}, \quad x_D = 1 + \frac{2u_1}{a_1^3} \tag{26}$$

In the case that it is supersonic at the end of the tube and the length of the shock-tube $x_l = L/l \leq x_D$ (l, L are the length of the high pressure section and the shock-tube respectively), for given initial values of regions (1) and (4), the entire flow field in the shock-tube can be obtained by using the equations for regions (2), (3), (5) and (7) as described above. Our experimental condition satisfied the conditions that the flow was supersonic at the end of the tube and $x_l \leq x_D$. Therefore, the above equations can be used to calculate the distribution of each parameter when the shockwave reaches the end of the tube (Figure 3(a)). Then the variations of the flow parameters at the end of the tube were converted from the time beginning with the breaking of the membrane $\tau = \bar{t}/(l/a_0)$ to the time $t = \bar{t}/(D/a_0)$. From the figure it can be seen that, if we let $x_L = 13$, then the calculated time of the arrival of the shockwave at the end of the tube $\tau_L = 4.065$, $\tau_1 = 5.511$, $\tau_2 = \cancel{6.065}\ 6.665$, and $\tau_3 = 7.5$. Based on this, we can also deduce

the relation between the dimensionless time t and τ to be

$$t = (\tau - \tau_L)(l/D) = (\tau - 4.065) \cdot 2$$

Therefore, when $\tau = \tau_L$, $t = 0$; $\tau = \tau_1$, $t = t_1 = 2.89$; $\tau = \tau_2$, $t = t_2 = 5.2$; $\tau = \tau_3$, $t = t_3 = 6.87$.

Figure 3a

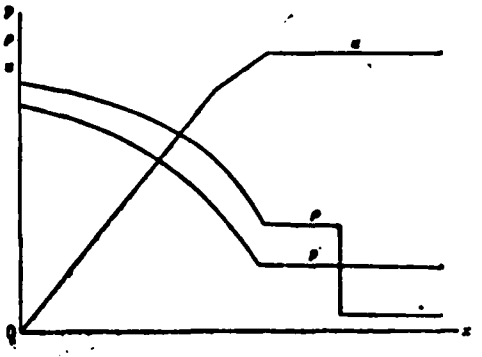

The practical procedure used in this paper to determine the boundary conditions at the end of the tube for numerical computations is: Starting at t = 0, the variation of each parameter at the end of the tube with time is:

1) when $0 \leqslant t < t_1$, it belongs to region (2):
$p_2 = 10$, $u_2 = 2.1775$, $\rho_2 = 3.81$

2) when $t_1 \leqslant t < t_2$, it belongs to region (3):
$p_3 = 10$, $u_3 = 2.1775$, $\rho_3 = 31.38$, $a_3 = 0.5646$

3) when $t_2 \leqslant t < t_3$, it belongs to region (7):
$u = 5(a-0,129)$

The variation of a(t) is obtained from Equation (22) and by noticing $\tau = (t+8.13)/2$:

$$t = 2\left[\bar{\tau}(a) + \frac{13 - \bar{x}(a)}{6a - 0.645}\right] - 8.13 \qquad (27)$$

where the expressions for $\bar{\tau}(a)$ and $\bar{x}(a)$ are obtained from the equation of CF after substituting the value $a = a_3 - (u_3/5) = 0.129$ into Equations (20) and (21), i.e.,

$$\tau = \bar{\tau}(a) = (0.3626 + 0.1903a - 0.475a^2)/a^3 \qquad (21')$$

$$z = \bar{z}(a) = (a - 0.129)\left[5\bar{\tau}(a) - \frac{a^2 + 0.129a + 0.4917}{a^3}\right] \qquad (22')$$

For convenience in using the computer, after calculating the numerical relationship between a and t for Equation (27), it is not difficult to obtain an approximate equation as follows:

$$a = 0.6563 - 0.01766t, \quad u = 2.6365 - 0.0883t \qquad (28)$$

The density ρ and pressure p are calculated using Equations (15) and (16).

4) When $t \geqslant t_3$, it belongs to region (6). Using x = 13 and $\tau = (t+8.13)/2$ to substitute into Equations (20) and (21), we find that the variations of u and a with time are as follows:

$$t = [3\xi^4 - 6(a^2 + 1)\xi^2 + 3a^4 + 2a^2 + 3]/(4a^3) - 8.13 \qquad (29)$$

$$13 = \xi[15\xi^4 - (26a^2 + 30)\xi^2 + 3a^4 + 6a^2 + 15]/(8a^3) \qquad (30)$$

From Equation (30) ξ and a can be solved. By substituing them into Equation (29), the corresponding t value can be computed. After performing the numerical calculations, the approximate equation can then be found for convenience in using the computer. In order to further improve the approximation, the approximate equation is chosen by sections as follows:

$$\left.\begin{aligned} a &= 0.5341 + 0.001588t - 0.0002123t^2 \\ u &= 3.285 - 0.2248t + 0.00611t^2 \end{aligned}\right\} \text{当 } 6.87 \leqslant t \leqslant 12.7 \text{ 时} \qquad (31)$$

$$\left.\begin{aligned} a &= 0.5709 - 0.004425t + 0.00003313t^2 \\ u &= 2.781 - 0.1423t + 0.002739t^2 \end{aligned}\right\} \text{当 } 12.7 < t \leqslant 18.61 \text{ 时} \qquad (32)$$

$$\left.\begin{aligned} a &= 0.5726 - 0.004573t + 0.00003604t^2 \\ u &= 2.1165 - 0.07136t + 0.0008482t^2 \end{aligned}\right\} \text{当 } 18.61 < t \leqslant 33.43 \text{ 时} \qquad (33)$$

$$\left.\begin{aligned} a &= 0.5528 - 0.003405t + 0.00001884t^2 \\ u &= 1.433 - 0.02933t + 0.000203t^2 \end{aligned}\right\} \text{当 } 33.43 < t \leqslant 57.31 \text{ 时} \qquad (34)$$

After a and u are solved, then the corresponding ρ and p are derived from Equation (15). The variations of various parameters at the end of the tube with time are shown in Figure 3(b).

It should be noticed that when t = 57.31, $\frac{u}{r}$ = 5, ξ = 0.4195 = a. Therefore, when t > 57.31, a subsonic flow begins to appear at the end of the tube. The outside of the tube would influence the inside, and the solution for region (6) becomes unapplicable. Henceforth, the computation carried out in this paper will not exceed a maximum time period t = 57.31.

3. Initial conditions

When t = 0, with the exceptions that $\rho_2 = 10$, $v_2 = 0$, $u_2 = 2.1775$, ~~2.1775~~ and ρ_2 = 3.81 at the end of the tube, in the remaining regions we will assume p = ρ = 1, and $u = v = 0$.

Figure 3(b)

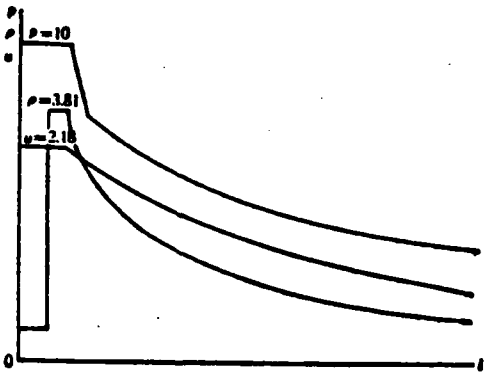

III. Difference equations

1. The format of difference for the internal points of a planar problem in gas dynamic equations [2]

A rectangular lattice is formed in a space coordinate system (x,y,t) with unit length Δx = h_1, Δy = h_2 and Δt = τ. Let the parameter A at a lattice point with coordinates (mh_1, lh_2, nτ)

be expressed as $A^{n}_{m,l}$. Furthermore, let us use the abbreviation A for it. In addition, let us decide to ignore all the other parameters with the same indices m,n,l. The set of gas dynamic equations after taking the fictitions viscosity into consideration can be transformed into the following set of difference equations:

$$f^{n+1} = f^{n} - \frac{k_1}{2}(F_{m+1} - F_{m-1}) - \frac{k_2}{2}(G_{l+1} - G_{l-1}) + \frac{1}{2}[\alpha_{m+\frac{1}{2}}(f_{m+1} - f_m) - \alpha_{m-\frac{1}{2}}(f_m - f_{m-1})] + \frac{1}{2}[\beta_{l+\frac{1}{2}}(f_{l+1} - f_l) - \beta_{l-\frac{1}{2}}(f_l - f_{l-1})] \qquad (35)$$

where the definitions of f,F and G are shown in Equations (2)-(4) and

$$\alpha_{m\pm\frac{1}{2}} = \frac{1}{2}(\alpha_{m\pm1} + \alpha_m), \quad \beta_{l\pm\frac{1}{2}} = \frac{1}{2}(\beta_{l\pm1} + \beta_l) \qquad (36)$$

Furthermore, $k_1 = \tau/h_1$, $k_2 = \tau/h_2$, $h_2/h_1 = \mathrm{tg}\psi$ α and β are defined as:

$$\alpha = \omega\sigma\sin^2\psi, \quad \beta = \omega\sigma\cos^2\psi \qquad (37)$$

where $\sigma = k(q + a)$, $k = \sqrt{k_1^2 + k_2^2}$, $q = (u^2 + v^2)^{1/2}$, $a = \sqrt{p/\rho}$ σ is called the Courant number at the nodal point of the lattice, ω is the stabilization constant and the stabilization condition of the difference equation requires [2]:

$$\sigma \leq \omega \leq 1/\sigma \qquad (38)$$

Since the stabilization condition (38) is valid at any lattice point under any condition, we can let $\sigma_0^* = \max \sigma_{m,l}^n$. If $\sigma_0^* \leq 1$ then the following equation must also be valid:

$$\sigma_0^* \leq \omega \leq 1/\sigma_0^* \qquad (39)$$

In the numerical computation of the computer, it can be determined that each level has the same σ_0 value. Based on the equation

$$k = \sigma_0/(q + a)_{max} \qquad (40)$$

the corresponding value of k at each level can be obtained. Since the values of h_1 and h_2 have been selected, the corresponding τ

value at this level can then be determined. Thus τ is selected. Any ω which satisfied $\sigma_i^* < \omega < 1/\sigma_i^*$ must also satisfy the condition $\sigma < \omega < 1/\sigma$ at any nodal point in the lattice at the same level. In the actual numerical computation, the selected value of σ_o at every level is the same constant value and the selected value of ω is also the same for all levels. But at every nodal point of the lattice at every level the value of σ is different which is determined by the equation $\sigma = k(q + a)$. The choice of τ in the machine is automatic.

2. <u>The format of difference at the boundary point in a planar problem</u>

From the difference format of internal point discussed in the previous section, it is understood that the calculation procedure uses the known parameters at five points (M,l), (M,$l \pm 1$) and ($m \pm 1$, l) at nth level to compute the unknown parameters (u,v, p,ρ) at point (m,l) of level n + 1. Equation (35) does not apply to boundary points. Some modification is necessary with regard to the difference format of the boundary points.

For horizontal solid wall (including horizontal symmetric axis) and vertical solid wall, we adopted the method which transfers the boundary difference format into the difference format for internal points. The actual procedure is: For horizontal solid wall, assuming that the index number is l in the y-direction of the solid wall and then sending $v_{l\pm1}$ to the unit of $v_{l\mp1}$ and then changing sign. For the other parameters $p_{l\pm1}, \rho_{l\pm1}, u_{l\pm1}$, their original values are transferred to $p_{l\mp1}, \rho_{l\mp1}, u_{l\mp1}$ respectively. This method in essence is to reflect the value of the $l \pm 1$ row into mirror image to the $l \mp 1$ row. After a row of points is generated, the original horizontal solid wall boundary can be considered as internal points. Computation can be carried out using the internal point difference format Equation (35). Similarly,

mirror reflection is made for the vertical solid wall which is to transfer $u_{m\pm1}$ to $u_{m\mp1}$ with a sign change and to transfer the original values of the other parameters.

3. Difference format of a slant wall

Generally ~~Geneally~~, the difference format of a slant wall will attempt to make the slant wall to coincide with the diagonal line of the difference lattice. Thus, we can rotate the slant wall by an angle ψ to transform the slant wall into a "horizontal" solid wall. After the difference format of this "horizontal" solid wall is written, we can then transfer the coordinate system to obtain the difference format of the slant wall:

$$\vec{f}^{n+1} = \vec{f}^{n} - \frac{k_1}{2}\cos\psi(\vec{F}_{m+1,l+1} - \vec{F}_{m-1,l-1}) - \frac{k_2}{\cos\psi}(\cos^2\psi\vec{G}_{m,l+1} + \sin^2\psi\vec{G}_{m-1,l}) + \frac{\cos^2\psi}{2}[(a_{m+\frac{1}{2},l+\frac{1}{2}}(\vec{f}_{m+1,l+1} - \vec{f}_{m,l}) - a_{m-\frac{1}{2},l-\frac{1}{2}}(\vec{f}_{m,l} - \vec{f}_{m-1,l-1})] \quad (41)$$

$$\vec{f} = \begin{pmatrix} \rho \\ \rho\tilde{u} \\ \rho\tilde{u}^2 + \frac{25}{7}p \end{pmatrix}, \quad \vec{F} = \begin{pmatrix} \rho\tilde{u} \\ \frac{5}{7}p + \rho\tilde{u}^2 \\ \rho\tilde{u}^3 + 5p\tilde{u} \end{pmatrix}, \quad \vec{G} = \begin{pmatrix} \rho\tilde{v} \\ \rho\tilde{u}\tilde{v} \\ (\rho q^2 + 5p)\tilde{v} \end{pmatrix} \quad (42)$$

Symbols with the "~" sign indicate that they are the parameters in the $(\tilde{x},\tilde{y})$ coordinate system which is formed by rotating the original coordinate system by an angle ψ with $\tilde{x}$ axis parallel to the slant wall and $\tilde{y}$ axis perpendicular to the slant wall. Their relations with those in the original coordinate system (x,y) are:

$$\tilde{u} = u\cos\psi + v\sin\psi, \quad \tilde{v} = -u\sin\psi + v\cos\psi \quad (43)$$

On the slant wall $\tilde{v} = 0$. Substituting this into the above equation, we get

$$u = \tilde{u}\cos\psi, \quad v = \tilde{u}\sin\psi \quad (44)$$

Based on the above equations, the values of parameters p, ρ, u, and v on the slant wall can finally be obtained.

4. The difference format in axial symmetry problems

The coordinate x represents the direction of the symmetric axis and the coordinate y axis represents the direction perpendicular to the symmetric axis. After adding another "$-\tau\psi$" term to the planar difference format, its internal point difference format is

$$f^{n+1}_{m,l} = f^{n}_{m,l} - \frac{k_1}{2}(F_{m+1,l} - F_{m-1,l}) - \frac{k_2}{2}(G_{m,l+1} - G_{m,l-1}) - \tau\Psi$$
$$+ \frac{1}{2}[\alpha_{m+\frac{1}{2},l}(f_{m+1,l} - f_{m,l}) - \alpha_{m-\frac{1}{2},l}(f_{m,l} - f_{m-1,l})]$$
$$+ \frac{1}{2}[\beta_{m,l+\frac{1}{2}}(f_{m,l+1} - f_{m,l}) - \beta_{m,l-\frac{1}{2}}(f_{m,l} - f_{m,l-1})] \qquad (45)$$

where the definitions of f, F, G and Ψ are shown in Equations (2)-(5). However, on the symmetric axis, because $y \to 0$ and $v \to 0$, the difference format is

$$f^{n+1}_{m,l} = f^{n}_{m,l} - \frac{k_1}{2}(F_{m+1,l} - F_{m-1,l}) - 2k_2 G_{m,l+1} + \frac{1}{2}[\alpha_{m+\frac{1}{2},l}(f_{m+1,l} - f_{m,l})$$
$$- \alpha_{m-\frac{1}{2},l}(f_{m,l} - f_{m-1,l})] + \beta_{m,l+\frac{1}{2}}(f_{m,l+1} - f_{m,l}) \qquad (46)$$

IV. Analysis of the computed results

We have computed four different conditions: Axial symmetric flow with vertical barrier wall without ground; two-dimensional planar flow with slant wall of actual dimensions with ground; and two-dimensional planar flow within two small areas with ground and slant wall. The objectives of the first three computations are to find the correction coefficients of the three-dimensional effect and the ground reflection effect. The last computation was done to examine the influence of the choice of the lattice boundary on the calculated result.

In computation, the values of the top and bottom boundary points at the end of the tube should be $u = v = 0$. The variations of p and ρ values with time should be the same as the values of the points inside the tube. In the meantime, please notice that inside the computed area it is a free boundary which is that before the shockwave propagates through p and ρ and 1 and u and v are 0 at the boundary. After the shockwave arrived, the following simple extrapolation method is adopted: Transferring all the computed parameter values of row l at level n to the positions of the corresponding points in row $l+1$. The value of free boundary in row l at level n+1 can thus be computed. Here l is the maximum number of lattice point in the computation in the y direction.

Based on the above computation method, some of the results are shown in Figures 4-6. The pressure distribution of the axial symmetric flow with vertical barrier wall is shown in Figure 4. After the shockwave has traveled through the end of the tube, the diffracted shockwave propagating forward will create a normal reflection when it collides with the vertical barrier wall. This normally reflected shockwave will also be compressed by the high pressure gas flow from the end of the tube. These phenomena are consistent with the experimental results [1].

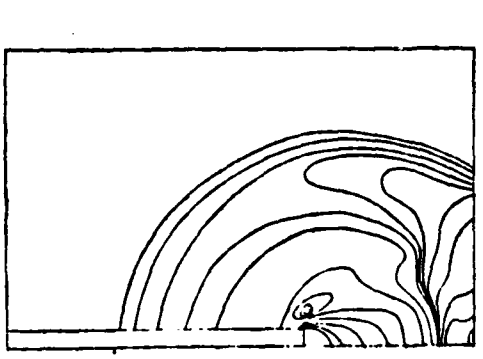

Figure 4. Axial symmetric condition
($\rho_{11} = 10 kg/cm^3$, $\tau = 4.32$, $n = 150$)

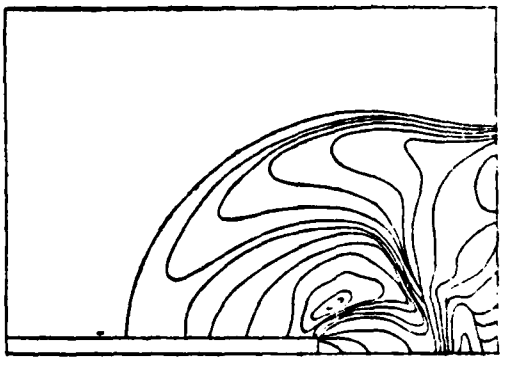

Figure 5. Plane condition
($\rho_{11} = 10 kg/cm^3$, $\tau = 4.43$, $n = 150$)

The pressure distribution of the planar flow with a vertical barrier wall is shown in Figure 5. Comparing the shockwave diffraction pattern of the axial symmetry flow (Figure 4) and planar flow (Figure 5) at the same time, it can be known that the shockwave velocity of the planar flow is faster than that of the axial symmetric flow. This explains that the induced pressure field by the axial symmetric flow is less than that induced by the planar flow.

The computed result of the shockwave climbing a 45° tilted wall (Figure 6) and the observed wave series diagram [1] are also consistent.

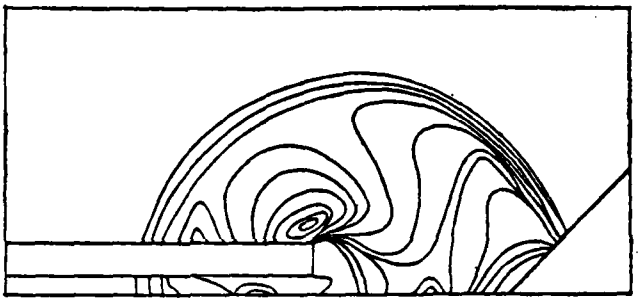

Figure 6. Planar condition (ρ_{st} = 10kg/cm², τ = 3.00, α = 100)

Based on the calculated data using the axial symmetry and vertical barrier wall method, we are drawing the variations of the over-pressure with the distance from the end of the tube radially at 90° and 150° angles (Figure 7). They are also more or less consistent with the results of the measurement of the over-pressure.

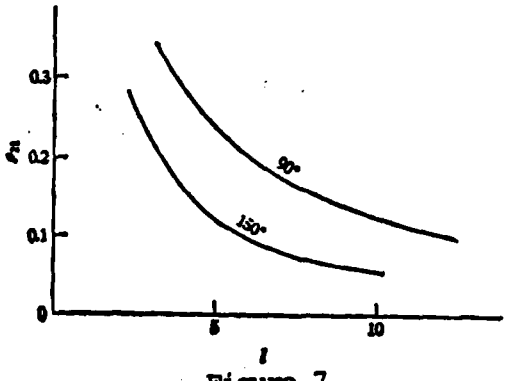

Figure 7

The pressure variations with time are drawn (Figure 8) for three fixed points which are 6m high from the ground at 45°, 60° and 90° angles in the radial direction for the planar computation condition. The effect of the slant wall on the reflected wave almost cannot be noticed. We have made measurements in the model experiment at 90° in the radial direction without discovering any effect of the slant wall on the reflected wave. This is consistent with the computed result.

We are most interested in the diffraction pressure on the rear wave at 150°C in the radial direction. The actual computed result after taking the correction coefficient of the three-dimensional effect into consideration indicated that the over-pressure of air at the end of the tube is 10 kg/cm^2 and the free diffraction over-pressure at the corresponding point is 0.06. The model experiment and actual on the spot experiment values are approximately 0.0645. This again explains that the computed value is consistent with the experimental value.

From the pressure distribution diagrams 4-6, we noted the existence of a low pressure nucleus region and the distribution of equi-pressure lines surrounding this nucleus at the upper side out of the end of the tube. It is equivalent to a whirlpool. This is also similar to the rotating ring observed experimentally [1] although the position of the two is slightly different.

We wish to thank comrades Liu Shijia and Wang Ruzhi for their assistance and support in this work. Comrades Shaojin Chin and Wu Fengyi also participated in the programming of this work.

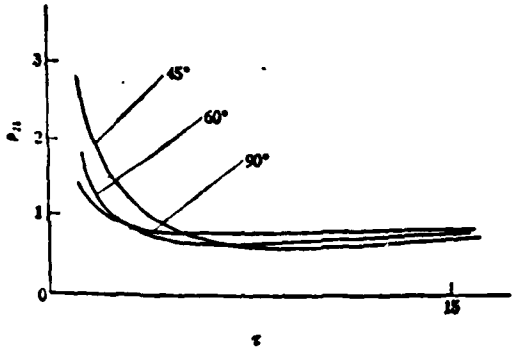

Figure 8

REFERENCES

1. Wei Zhong-lei, Wang Bing-zheng, Zhang Jun-xiu, Acta Mechanica Sinica, 1 (1979), pp 70-73

2. Rusanov, V.V. ZhVMMF, 1 (1961), 267-279

THE NUMERICAL COMPUTATION FOR DIFFRACTION AND REFLECTION OF A TRAVELLING SHOCK WAVE FROM AN OPEN END OF A SHOCK-TUBE

Du Xun Wei Zhong-lei Li Wen-xuan Wang Jia-jun

(Beijing University)

Abstract

When a shock wave travells into atmosphere from an open end of a shock-tube, an over-pressure field is induced and wave diagrams of shock diffraction and reflection form immediately. In general, one can always compute the outflow problem by solving the unsteady two-dimensional gasdynamic equations. Computing this problem numerically, the authors take advantage of Eulerian coordinates, fictitious viscosity and finite difference method. In order to decide the boundary conditions for computation at the end of tube, first we find out analytical solution for the unsteady one-dimensional flow in a shock-tube, and then the variations of the velocity, pressure and density of the flow at the open end of the tube with time. The present numerical results are in agreement with the experiments.


FILME
8